

1 **Retrogressive thaw slumps temper dissolved organic carbon delivery to streams of the Peel Plateau,**
2 **NWT, Canada**

3

4 Cara A. Bulger^{1*}, Suzanne E. Tank¹, and Steven V. Kokelj²

5

6 ¹Department of Biological Sciences, University of Alberta, Edmonton, AB, Canada, T6G 2E9

7 ²Northwest Territories Geological Survey, Government of the Northwest Territories, Yellowknife, NT,
8 Canada

9 *Author for correspondence: cara.bulger@gmail.com

10

11

12 **Abstract**

13 In Siberia and Alaska, permafrost thaw has been associated with significant increases in the delivery of
14 dissolved organic carbon (DOC) to recipient stream ecosystems. Here, we examine the effect of
15 retrogressive thaw slumps (RTS) on DOC concentration and transport, using data from eight RTS features
16 on the Peel Plateau, NT, Canada. Like extensive regions of northwestern Canada, the Peel Plateau is
17 comprised of thick, ice-rich tills that were deposited at the margins of the Laurentide Ice Sheet. RTS
18 features are now widespread in this region, with headwall exposures up to 30 m high, and total
19 disturbed areas often exceeding 30 ha. We find that intensive slumping on the Peel Plateau is universally
20 associated with decreasing DOC concentrations downstream of slumps, even though the composition of
21 slump-derived dissolved organic matter (DOM; assessed using specific UV absorbance and slope ratios)
22 is similar to permafrost-derived DOM from other regions. Comparisons of upstream and downstream
23 DOC flux relative to changes in total suspended solids suggest that the substantial fine-grained
24 sediments released by RTS features may sequester DOC. Runoff obtained directly from within slump
25 features, above entry into recipient streams, indicates that the deepest RTS features, which thaw the
26 greatest extent of buried, Pleistocene-aged glacial tills, have the lowest runoff DOC concentrations when
27 compared to upstream, un-disturbed locations. In contrast, shallower features, with exposures that are
28 more limited to a relict Holocene active layer, have within-slump DOC concentrations more similar to
29 upstream sites. Finally, fine-scale work at a single RTS site indicates that temperature and precipitation
30 serve as primary environmental controls on above-slump and below-slump DOC flux, but that the
31 relationship between climatic parameters and DOC flux is complex for these dynamic thermokarst
32 features. These results demonstrate that we should expect striking variation in thermokarst-associated
33 DOC mobilization across Arctic regions, but that within-region variation in thermokarst intensity and
34 other landscape factors is also important for determining biogeochemical response. An understanding of
35 landscape and climate history, permafrost genesis, soil composition, the nature and intensity of
36 thermokarst, and the interaction of these factors, is critical for predicting changes in land-to-water

Deleted: continental ice sheet

Deleted: a conservative tracer

Deleted: slumping

Deleted: on this landscape

Deleted: feature

42 carbon mobilization in a warming Arctic.

43

Deleted: circumpolar world

45 **1. Introduction**

46 Anthropogenic climate change is significantly affecting the Canadian Arctic cryosphere (IPCC,
47 2014). Temperature increases in Arctic regions are predicted to be at least 40% greater than the global
48 mean, while precipitation is also expected to increase significantly in many locations (IPCC, 2014). The
49 resulting degradation of permafrost is forecast to have wide-ranging effects, because thawing has the
50 potential to greatly alter the physical, chemical, and biological functioning of landscapes (Frey and
51 McClelland, 2009; Khvorostyanov et al., 2008a, 2008b; Kokelj et al., 2017b; Schuur et al., 2008, 2013). In
52 particular, permafrost acts as a long term storage medium for solutes and sediments, and as a barrier to
53 the participation of permafrost-sequestered constituents within active biogeochemical cycles (Frey and
54 McClelland 2009; Vonk et al. 2015b). Consequently, permafrost thaw can enhance linkages between
55 terrestrial and aquatic systems, via increased transport of terrestrial compounds from land to water
56 (Kokelj et al. 2013; Tanski et al., 2016; Vonk et al., 2015b). Given that northern circumpolar permafrost
57 stores of carbon are estimated to be almost double that of the atmospheric carbon pool (Hugelius et al.,
58 2014), there is great potential for large increases in carbon mobilization as a result of permafrost thaw
59 (Schuur et al., 2015). Within this context, the mobilization of dissolved organic carbon (DOC) from
60 previously frozen soils is of particular interest, because DOC acts as the primary substrate for the
61 microbially-mediated mineralization of organic carbon to carbon dioxide (Battin et al., 2008), while also
62 serving as the primary vehicle for the delivery of terrestrial carbon to the Arctic Ocean (Dittmar and
63 Kattner, 2003; Holmes et al., 2012; Spencer et al., 2015). As a result, the implications of thaw-mediated
64 DOC mobilization may range from effects on the permafrost-carbon feedback, to the ecological and
65 biogeochemical functioning of streams, rivers, and the nearshore ocean (e.g. Fritz et al. 2017; Tank et
66 al., 2012b; Vonk et al., 2015b).

67 Permafrost thaw can manifest in many different forms, ranging from an increase in active layer
68 thickness and terrain subsidence, to thermokarst features that significantly reconfigure the physical
69 structure of the landscape. Of these, thermokarst has the potential to rapidly expose significant

Deleted: (IPCC, 2014)

Deleted: (Walsh et al., 2011)

Deleted: (McGuire et al., 2009)

Deleted: s

Deleted: s

Deleted: increasing

Deleted: global

Deleted: transport

Deleted: land to water

Deleted: ; Spencer et al., 2015

Deleted: . Dissolved organic carbon also forms the majority of total organic carbon flux in most Arctic rivers (Spencer et al., 2015), and is thus the primary vehicle for the delivery of terrestrial carbon to the Arctic Ocean

84 quantities of previously-frozen soils to biological and chemical processing (Abbott et al., 2014, 2015;
85 Kokelj and Jorgenson, 2013; Malone et al., 2013; Tanski et al. 2017). One of the most conspicuous
86 manifestations of thermokarst is the retrogressive thaw slump (RTS; Fig. 1), which develops as a result of
87 mass wasting, in ice-rich glacial deposits across northwestern Canada, Alaska, and western Siberia
88 (Kokelj et al., 2017b), and in Yedoma regions of Alaska and Siberia (Murton et al., 2017). Thaw slumps
89 are widespread throughout glaciated terrain in the western Canadian Arctic (Kokelj et al., 2017b; Lantuit
90 et al. 2012), including on the Peel Plateau (Lacelle et al., 2015). These dynamic landforms develop via
91 the ablation of an ice-rich headwall and – through the coupling of geomorphic and thermal processes –
92 are particularly efficient at thawing thick zones of ice-rich permafrost and translocating large volumes of
93 sediment from slopes to downstream environments (see Fig. 1). RTS features remain active for decades
94 (Lantuit et al. 2012). They typically stabilize following sediment accumulation at the base of the
95 headwall (Kokelj et al., 2015), but can reactivate causing thaw within the scar zone, and upslope
96 expansion of the disturbance (Kokelj et al., 2013; Lantuit and Pollard, 2008). During periods of activity,
97 thawed materials accumulate as a saturated slurry in the slump scar zone (see Fig. 1b) and are
98 translocated downslope by mass flow processes, which are accelerated by meltwater- and rainfall-
99 induced saturation (Kokelj et al. 2015). During active and stabilized periods, surface runoff can also
100 remove solutes and suspended sediment from the thawed substrate to downstream environments.
101 Although variation in temperature, precipitation and solar radiation have been correlated with
102 development rates and growth of RTS features (Kokelj et al., 2009, 2013, 2015; Lacelle et al., 2010;
103 Lewkowicz, 1986, 1987), we know little about how these and other environmental drivers might control
104 permafrost-DOC dynamics at the individual-slump to small watershed scale.

Deleted: that insulates the ground ice and arrests thaw

Deleted: retrogressive thaw slumps

105 On the Peel Plateau, an individual thaw slump can impact tens of hectares of terrain, displace
106 hundreds of thousands of cubic meters of sediments, and significantly alter surface water sediment and
107 solute loads (Kokelj et al., 2013; Malone et al., 2013), and thus downstream ecosystems (Chin et al.,
108 2016; Malone et al., 2013). The magnitude of these disturbances and their cumulative impacts is great

Deleted: s

Deleted: commonly

Deleted: downslope

114 enough to alter solute loads in the Peel River (70,000 km² watershed area; Kokelj et al., 2013), even
115 though only a small portion of that river's total catchment area (<1%) is influenced by thermokarst
116 (Kokelj et al., 2017b; Segal et al., 2016). This contrasts with many other thaw-affected regions, where
117 increases in solute loads following permafrost disturbance can be transient (e.g., limited to spring
118 freshet) and have little overall effect on annual solute fluxes (for example, in High Arctic regions affected
119 by active layer detachments; Lafrenière & Lamoureux, 2013). In addition, permafrost thaw on the Peel
120 Plateau is notable in that it exposes vast quantities of mineral-rich glacial till, which is overlain by a
121 relatively shallow layer of slightly more organic-rich soils (Duk-Rodkin and Hughes, 1992; Kokelj et al.
122 2017a). Although this till-associated, RTS-susceptible landscape type is found across the Laurentide and
123 Barents-Kara glacial margins of Canada, Alaska, and Siberia (Kokelj et al. 2017b), it contrasts with
124 regions of Alaska and eastern Siberia that are either Yedoma-rich or were patchily glaciated during the
125 late Pleistocene, which have been common focus points for study of permafrost-DOC interactions to
126 date (Abbott et al., 2014, 2015; Drake et al., 2015; Mann et al., 2012; Vonk et al., 2013b).

127 Thermokarst has been documented to enhance DOC concentrations in recipient aquatic
128 ecosystems in several Arctic regions (Frey and McClelland, 2009; Tank et al., 2012a; Vonk et al., 2013a;
129 Vonk and Gustafsson, 2013). In Alaska, streams draining thaw slumps have higher DOC concentrations
130 than un-affected systems across various terrain types (2-3 fold increase; Abbot et al., 2014), while in
131 eastern Siberia the DOC concentration in runoff from thawing Yedoma is considerably greater than
132 concentrations in recipient river systems (~30-fold elevation; Spencer et al. 2015). However, multiple
133 factors, including variable carbon content in permafrost soils (Hugelis et al. 2014) and variation in
134 ground ice type and volume (Fritz et al. 2015), may affect DOC release from permafrost. In regions where
135 thermokarst transports fine-grained sediments to aquatic systems, sorption processes may also be
136 important, because dissolved organic matter (DOM) can readily sorb to mineral soils (e.g., Kothawala et
137 al. 2009). Sorption to mineral sediments can cause DOM to be rapidly removed from solution in stream
138 systems (Kaiser and Guggenberger, 2000; Kothawala et al. 2009; McDowell, 1985), while also enabling

Deleted: e

Deleted: permafrost

Deleted: landscape type is found across glaciated permafrost terrains of the circumpolar North

Deleted: h

Deleted: e.g.,

Deleted: and

Deleted: In several Arctic regions, p

Deleted: ermafrost thaw, including t

Deleted: ,

Deleted: For example

Deleted: in Alaska

Deleted: in eastern Siberia

Deleted:

Deleted: with

Deleted: thaw

Deleted: This

Deleted: rapid process

Deleted: is largely regulated by the chemical composition and clay content of mineral sediments (Kothawala et al. 2009), and

Deleted: .The DOM-mineral complex can be an important mechanism for

161 the downstream transport and continued sequestration of organic carbon (Hedges et al., 1997). This
 162 process may be particularly important for regulating DOC dynamics in glacial margin landscapes such as
 163 those in the western Canadian Arctic, where a predisposition to thaw slumping results in an abundance
 164 of thermokarst-related slope disturbances which mobilize fine-grained glacial sediment stores to
 165 downstream systems (Kokelj et al., 2017a, 2017b; Lantuit et al. 2012; Rampton, 1988). Although the
 166 mechanisms governing the thaw-mediated transport of DOC from land to freshwater seem likely to
 167 differ in till-dominated landscapes when compared to other regions studied to date, little is known
 168 about the downstream consequences of permafrost thaw for carbon biogeochemistry in regions such as
 169 the Peel Plateau.

Deleted: Sorption

Deleted: processes

Deleted: transport

Deleted: the glaciated

Deleted: landscape

Deleted: thermokarst

Deleted: effectively

170 The objective of this study is to quantify how RTS features affect the concentration and
 171 composition of DOC across a series of slump-affected streams on the Peel Plateau, and to examine how
 172 observed variation in slump morphology affects DOC dynamics in slump-affected downstream
 173 environments. We further investigate how short-term variation in precipitation, temperature, and solar
 174 radiation affect DOC delivery from land to water, using measurements of DOC flux above and below a
 175 single RTS feature. We target the thermokarst-sensitive Peel Plateau for this work, which is
 176 characteristic of till-rich, glacial margin landscapes throughout Canada, Alaska, and Siberia (Kokelj et al.
 177 2017b). By comparing our results to those from other regions, this allows us to consider how broad
 178 variation in permafrost soil composition, permafrost genesis, and Quaternary history may drive variation
 179 in land-freshwater DOC dynamics across divergent regions of the Arctic affected by permafrost thaw.

Deleted: In this study, we

Deleted: on the Peel Plateau

Deleted: within

Deleted: recipient stream systems

Deleted: , to explore how DOC mobilization from land to water is affected by thermokarst in this region.

Deleted: , to explore the drivers of temporal variation in DOC flux

Deleted: specifically

Deleted: se

Deleted: glacial deposits

Deleted: are

Deleted: large portions

Deleted: of the circumpolar Arctic, to explicitly

Deleted: s

Deleted: ,

Deleted: influence

Deleted: variability

Deleted: permafrost-DOC interactions

Deleted: vast

Deleted: Arctic regions. The study results broaden our understanding of land-water carbon mobilization in permafrost terrain, and indicate that slumping on the Peel Plateau may act to temper the flux of DOC within this landscape, via mineral-carbon interactions. These findings also underline the importance of landscape characteristics and geological inheritance for determining the biogeochemical effects of thermokarst, particularly as hillslope thermokarst intensifies across many Arctic regions (Kokelj et al., 2017b).

182 2 Study Site

183 2.1 General study site description

184 Our study was conducted on the Peel Plateau, situated in the eastern foothills of the Richardson

220 Mountains, NWT, Canada, in the zone of continuous permafrost (Fig. 1a). The fluviially-incised Plateau
221 ranges in elevation from 100 to 650 masl. The region was covered by the Laurentide Ice Sheet (LIS) for a
222 brief period (a maximum of 2,000-3,000 years) 18,500 cal yr BP (Lacelle et al., 2013). The bedrock of the
223 region is Lower Cretaceous marine shale from the Arctic River formation (Norris, 1984) and siltstone
224 overlain by Late Pleistocene glacial, glacio-fluvial and glacio-lacustrine sediments (Duk-Rodkin and
225 Hughes, 1992), covered by a shallow organic layer. These Pleistocene deposits host ice-rich permafrost.
226 Radiocarbon dating in the region has placed the age of relict ground ice in the late Pleistocene epoch
227 (18,100 ± 60 ¹⁴Cyr BP; Lacelle et al., 2013). Upper layers of permafrost thawed during the early Holocene
228 and host younger, Holocene-aged organic materials (7890 ± 250 ¹⁴Cyr BP; Lacelle et al., 2013). These are
229 clearly delineated from deeper Pleistocene-aged permafrost by a thaw unconformity (Burn 1997; Fig. 1),
230 which developed when warmer climate during the early Holocene prompted the thawing of near-
231 surface permafrost and a regional increase in active layer thickness, enabling the leaching of soluble ions
232 and integration of organic matter into these previously thawed soils (see Fig. 1c-d). Subsequent
233 aggradation of permafrost due to gradual cooling has archived this notable stratigraphic variation in
234 geochemistry, organic matter content, and cryostructure (Burn 1997; Fritz et al. 2012; Kokelj et al.,
235 2002; Lacelle et al., 2014; Murton and French, 1994).

236 Ice-marginal glacial landscapes such as the Peel Plateau host thick layers of ice-rich
237 sediments, and thus have a predisposed sensitivity to climate-driven thaw slump activity (Kokelj et al.,
238 2017). On the Peel Plateau, slumping is largely constrained by the maximum extent of the LIS, because
239 the thick layers of ice-rich permafrost necessary for RTS activity are not present beyond its glacial limits
240 (Lacelle et al., 2015). Fluvial incision provides the topographic gradients necessary for thaw slump
241 development and RTS features are common; ranging in size from small, newly developing features,
242 which are relatively numerous, to those greater than 20 ha, which are rare (<5% prevalence; Lacelle et
243 al., 2015). The recent intensification of slumping on the Peel Plateau is driven in part by increasing air
244 temperatures and summer rainfall intensity (Kokelj et al., 2015). This intensification is also increasing the

Deleted: (Kokelj et al., 2016)

Deleted: (Catto, 1996)

Deleted: Laurentian

Deleted: Carbon

Deleted: and ¹⁸O measurements

Deleted: have

Deleted: es

Deleted: is

253 thaw of the deepest layer of ice-rich, organic-poor, Pleistocene-aged glacial till that underlie this
254 region. The pattern of abundant thaw slump development across ice-marginal glaciated permafrost
255 landscapes extends from the Peel Plateau across the western Canadian Arctic, and persists at
256 continental scales (Kokelj et al., 2017b).

257

258 2.2 Regional climate

259 The regional climate is typical of the subarctic with long, cold winters and short, cool summers.
260 Mean annual air temperature (1981-2010) at the Fort McPherson weather station (Fig. 1a) is -7.3 °C
261 with average summer (June-August) temperatures of 13.3 °C (Environment Canada, 2015). A warming
262 trend of 0.77 °C per decade since 1970 has been recorded; however these increases are most apparent
263 in the winter months (Burn and Kokelj, 2009). Our sample period spanned the thaw months of July and
264 August; average 1981-2010 temperatures for those months, recorded at Fort McPherson, are 15.2 and
265 11.8 °C, respectively, similar to temperatures at Fort McPherson during 2014 (15.6 and 11.6 °C), but
266 slightly higher than 2014 averages observed at a recently established meteorological station on the Peel
267 Plateau (Fig. 1a; 13.2 °C in July and 9.5 °C in August). Annual cumulative rainfall (1981-2010) at Fort
268 McPherson averages 145.9 mm, with July and August having the highest rainfall levels at 46.4 and 39.1
269 mm (Environment Canada, 2015). In 2014, rainfall for July and August was 71 and 121 mm at Fort
270 McPherson, and 128.7 and 170.7 mm on the Peel Plateau. This continues the trend for this region of
271 increasingly wet summers with numerous extreme rainfall events (Kokelj et al., 2015).

Deleted: more elevated, centrally-located meteorological station

Deleted: (Fig. 1a) during our study

Deleted: the

Deleted: weather station

Deleted: makes 2014 a cooler year than average, and

Deleted: ter

272

273 3 Methods

274 3.1 Slump site selection

275 Eight RTS features were selected from across the study region, using aerial surveys and previous
276 knowledge of features across this landscape (Fig. 1; Fig. S1; Table 1). Selected slumps possessed a debris
277 tongue that extended to the valley bottom and directly impacted a stream system. Sampling at each

284 slump occurred at three discrete locations: upstream, within-slump, and downstream of slump influence
285 (Fig. 1b). Upstream sites were trunk streams that connected with the slump flow path further
286 downstream, and were un-affected by any major geomorphic disturbance and thus representative of an
287 undisturbed, pristine environment. Within-slump sampling locations were locations of channelized
288 slump runoff within the scar zone or upper debris tongue. Downstream sampling locations were located
289 below the confluence of the sampled upstream flow and all within-slump runoff paths, and were chosen
290 to be representative of slump impact on aquatic ecosystems across the Peel Plateau landscape. In one
291 instance (Slump HD, August 17), a fluidized flow event between sampling events saturated the scar zone
292 and obliterated within-slump channelized surface flow. As a result, the within-slump sample taken at
293 this site was not representative of typical channelized slump runoff that characterized all other slump
294 sampling conditions, and has been discarded from all analyses.

295 A general classification of the slumps is difficult as these features are influenced by a diverse
296 range of geomorphic processes that vary in intensity over time (Table 1; Fig. S1). Three of the slumps
297 (FM4, FM2, FM3) are classified as ‘mega slumps’, characterised by areas greater than 5 ha, a headwall
298 greater than 4 m in height, and a debris tongue that connects the slope to the valley below (Kokelj et al.,
299 2013, 2015). Of these, FM4 possesses a headwall approximately 20 m in height, but ~~was~~ largely
300 stabilized in 2014, indicated by the small outflow, long, dry, and significantly revegetated debris tongue
301 (Fig. S1). FM2 is among the largest active slumps in the region, with a headwall 25-30 m high and visible
302 as a much smaller feature in air photos since 1944 (Lacelle et al. 2015). FM2 geochemistry and
303 geomorphology were previously described by Malone et al. (2013). Slump FM3, which was chosen for
304 our ‘environmental controls’ work (further described below) covers an area of approximately 10 ha, and
305 has a headwall of approximately 10 m in height and a debris tongue that extends nearly 600 m down
306 valley (Table 1). Headwall retreat rate at FM3 over a 20 year period has been calculated at 12.5 m yr⁻¹
307 (Lacelle et al., 2015). SD is the smallest and youngest slump that we studied, and was initiated when
308 diversion of a small creek caused lateral bank erosion. In 2014, the SD headwall was 2-4 m high with a

Deleted: substantial

Deleted: is currently

Deleted: T

Deleted: is

313 scar zone extending approximately 20m, and no defined debris tongue. The remaining slump sites (HA,
314 HB, HC, HD) were all well-developed active RTS features with headwalls similar to, or smaller than, FM3,
315 but with debris tongues much smaller in volume (Table 1). With the exception of SD, slump headwalls
316 exposed permafrost well below a thaw unconformity, indicating that Pleistocene-aged, unweathered
317 glacial materials were being thawed by the slump (Lacelle et al., 2013).

Deleted: that extends

Deleted: that are

Deleted: are

319 3.2 Field sampling and data collection

320 3.2.1 The effect of slumping on DOC and stream water chemistry

321 The majority of our sampling was conducted during the summer of 2014. Of the eight slumps
322 that were sampled, three were accessed from the Dempster Highway three times over the sampling
323 season, one (FM3; see also 3.2.2) was accessed twice from the highway, and four were accessed twice
324 via helicopter (Table 1). At each of the upstream, downstream, and within-slump sampling locations,
325 specific conductivity, pH, and temperature were recorded using a YSI Pro Plus multi-parameter meter.
326 Water samples were collected from directly below the stream surface into 1 L acid washed HDPE bottles
327 and allowed to sit in chilled, dark conditions for 24 hours to enable the considerable sediments in these
328 samples to partially settle out of suspension. Sample water was then filtered with pre-combusted
329 (475°C, 4 hours) Whatman GF/F filters (0.7 µm pore size). Filtered sample water was transferred into 40
330 mL acid washed, pre-combusted glass bottles for DOC analysis, or 60 mL acid washed HDPE bottles for
331 the analysis of absorbance and major ions. DOC samples were acidified with hydrochloric acid (1 µL mL⁻¹),
332 following Vonk et al. (2015b). The GF/F filters were retained for analysis of total suspended solids,
333 (TSS), Samples for stable water isotopes were collected directly from streams into acid washed 40 mL
334 HDPE bottles with no headspace and sealed. During summer 2016, samples were additionally collected
335 from a subset of slump locations (FM2, FM3, FM4 and SD) for the ¹⁴C signature of DOC at upstream and
336 within-slump sites. DO¹⁴C samples were collected in acid-washed polycarbonate bottles, allowed to
337 settle for 24 hours, and filtered using pre-combusted Whatman GF/F filters into pre-combusted glass

Deleted: At each slump, samples were collected at upstream, downstream, and within-slump locations.

Deleted: substantial

Deleted: All samples were refrigerated until analysis.

Deleted: sediment

Deleted: ?

Deleted: analysis

Deleted: analyses

Deleted: . Bottles were

Deleted: and refrigerated until analysis

Deleted: Field

Formatted: Superscript

Deleted: pre

Deleted: 1-2 L

354 media bottles with phenolic screw caps with butyl septa. All samples were refrigerated until analysis.
355 Absorbance samples were analyzed within 1 week of collection, cation samples within 4 months of
356 collection, and DOC (including ¹⁴C) samples within 1-2 months of collection. Samples for Fe and $\delta^{18}\text{O}$
357 were analyzed within 6 months of collection.

Deleted: Sample bottles were wrapped in aluminum foil and

Formatted: Superscript

358

Deleted: ¶

359 3.2.2 Environmental controls on DOC flux

360 To explore how environmental variables control the flux of DOC from RTS-affected streams, we
361 visited slump FM3 an additional 17 times beyond the sampling described above. This intensively-studied
362 site was chosen to be representative of active Peel Plateau slumps that are eroding Holocene- to
363 Pleistocene-aged sediments. During each visit, we measured discharge at the upstream and downstream
364 locations to calculate DOC flux, and collected upstream and downstream DOC concentration samples.
365 Downstream discharge was measured using an OTT C2 current meter at three locations across the small
366 stream and at 40% depth. Due to the shallow, low flow conditions at the upstream site, upstream
367 discharge was measured using the cross sectional method (Ward and Robinson, 2000). In both cases,
368 discharge was calculated as the product of velocity and stream cross-sectional area. Local daily climate
369 data were obtained from an automated meteorological station established in 2010 by the Government
370 of the Northwest Territories (Kokelj et al. 2015). The station is located within 2 km of slump FM3 (Fig.
371 1a) and is instrumented for the measurement of air temperature, rainfall, and net radiation.

Deleted: previously

372

373 3.3 Laboratory analyses

374 3.3.1 Major ions, dissolved organic carbon, $\delta^{18}\text{O}$ and DO^{14}C

375 Cation concentrations (Ca^{2+} , Mg^{2+} , Na^+) were analyzed on a Perkin Elmer Analyst 200 Atomic
376 Absorption Spectrometer at York University. A subset of collected samples were analyzed for total
377 dissolved Fe at the University of Alberta on an Inductively Coupled Plasma - Optical Emission
378 Spectrometer (Thermo Scientific ICAP6300), to allow for the correction of our Specific UV Absorbance

382 results (see below). DOC samples were analyzed on a Shimadzu TOC-V analyzer; DOC was calculated as
383 the mean of the best 3 of 5 injections with a coefficient of variation of <2%; the precision of a 10 mg L⁻¹
384 caffeine standard across all sample runs was 0.32 mg L⁻¹. A Picarro liquid water isotope analyzer was
385 used to measure $\delta^{18}\text{O}$ at the University of Alberta, following filtration (0.45 μm cellulose acetate,
386 Sartorius) into 2 mL autosampler vials (National Scientific), without headspace. The precision of our
387 $\delta^{18}\text{O}$ analysis is $\pm 0.2\%$. The radiocarbon signature of DOC was measured following extraction and
388 purification at the A.E. Lalonde AMS facility (University of Toronto) using a 3MV tandem accelerator
389 mass spectrometer (High Voltage Engineering) following established methodologies (Lang et al., 2016;
390 Palstra and Meijer, 2014; Zhou et al., 2015), and is reported with an error estimate of 1 σ .

Deleted: variance

Formatted: Superscript

Formatted: Superscript

Deleted: stable water isotope samples

392 3.3.2 Total suspended solids

393 Samples for TSS were filtered in the field for later analysis, ensuring that there was enough
394 sediment on the pre-combusted (475°C, 4 hours) and pre-weighed GF/F filters. Filters were stored
395 frozen, dried at 60°C for 8 hours, placed in a desiccator overnight and promptly weighed. TSS was
396 calculated as the difference in filter weight before and after sediment loading, divided by volume
397 filtered.

Deleted: sediments

Deleted: total suspended sediments (

Deleted:)

399 3.3.3 Dissolved organic matter spectral characteristics

400 DOM composition was assessed using absorbance-based metrics. A 5 cm quartz cuvette was
401 used to obtain UV-visible spectra data from 250-750 nm, using a Genesys 10 UV-Vis spectrophotometer.
402 A baseline correction was applied to eliminate any minor interference from particles $< 0.7 \mu\text{m}$ (Green
403 and Blough 1994). Specific UV absorbance at 254 nm (SUVA_{254}), which is correlated with DOM
404 aromaticity (Weishaar and Aiken, 2003), was calculated by dividing the decadal absorbance at 254 nm
405 (m^{-1}) by the DOC concentration (mg L^{-1}). SUVA_{254} values were corrected for Fe interference following
406 Poulin et al. (2014) using maximum Fe concentrations from laboratory analyses or as reported in Malone

Deleted: potential

Deleted: following

Deleted: &

Deleted: (

416 et al. (2013). Spectral slopes between 275 and 295 nm, and 350 and 400 nm ($S_{275-295}$, $S_{350-400}$) were
417 calculated following Helms et al. (2008), and are reported as positive values to adhere to mathematical
418 conventions. Slope ratios (S_R), which correlate with DOM molecular weight (Helms et al., 2008), were
419 calculated as the ratio of $S_{275-295}$ to $S_{350-400}$.

420

421 3.4 Statistical analyses and calculations

422 Statistical analyses were completed in R version 3.1.3 (R Core Team, 2015) using packages 'nlme'
423 (Pinheiro et al., 2015), 'lme4' (Zeileis and Hothorn, 2002), 'lmeSupport' (Curtin, 2015), 'car' (Fox and
424 Weisberg, 2011), and 'zoo' (Zeileis and Grothendieck, 2005). The effect of slumping on stream chemistry
425 and optical characteristics was assessed using linear mixed effects models in the 'nlme' package of R. For
426 each parameter, analyses were split into two separate models that included data for upstream and
427 downstream chemistry, and upstream and within-slump chemistry. We used this approach to separately
428 assess the effects of slumping downstream of slump systems, and to compare the composition of slump
429 runoff to nearby, pristine environments. For each analysis, we included slump location (see Table 1) as a
430 random effect, and considered models that either nested Julian date within the random effect of slump
431 location, or allowed Julian date to occur as a fixed effect. The best model was chosen using the Akaike
432 information criterion (AIC), and best-fit models were refit with a variance structure to ensure that model
433 assumptions were met. The variance structures varIdent (for within-slump site and slump location) and
434 varFixed (for Julian date) were used together (using varComb) and in isolation for this purpose (Zuur et
435 al., 2009). AIC values for the weighted and un-weighted models were again compared to choose a final
436 model of best fit for each analysis.

437 We used the high-frequency data from slump FM3 to assess how environmental conditions
438 (rainfall, temperature, solar radiation) and TSS affect DOC delivery to slump-affected streams. To do
439 this, we conducted multiple linear regressions, using AIC values to determine models of best fit
440 (Burnham and Anderson, 2002). To enable a specific assessment of environmental controls on

Deleted: systems

442 downstream DOC flux, upstream DOC flux was separated out into a distinct regression analysis, because
443 upstream DOC flux was strongly correlated with flux downstream, and therefore overwhelmed all
444 environmental variables in the downstream model. Models were tested for serial correlation using the
445 auto-correlation function, and models with variance inflation factors greater than 10 or significant
446 Durbin Watson test results (indicative of correlated variables; Durbin & Watson, 1950; Hair et al., 1995)
447 were discarded. Residuals were examined to ensure the model was a good fit for the data (Zuur et al.,
448 2009). We considered both time-of-sampling (0 h) and past (48, 72, and 120 h) environmental conditions
449 in our analyses. Because cumulative values for environmental variables (i.e. accumulated rainfall in the
450 previous 48, 72 and 120 h) showed a strong positive correlation to one another, we used temporally
451 shifted data (i.e. rainfall 48, 72 and 120 h prior to the DOC flux measurement) in the final model. Similar
452 models were also constructed to examine the effects of environmental drivers on DOC concentration.

Deleted: (ACF)

453 Differences in paired upstream-downstream measures of DOC flux and concentration at slump FM3
454 were also assessed using a Wilcoxon Signed Rank Test, a non-parametric analog to the paired-t test.

Deleted: Finally, d

455 Following our finding of decreasing DOC concentrations downstream of slumps (see Sections 4.1
456 and 5.1) we used data from slump FM3, where we have upstream, downstream, and within-slump DOC
457 concentration measurements, and upstream and downstream discharge measurements, to calculate a
458 mass balance for DOC across the three sampling locations. These data – available for all three locations
459 on two dates during the summer of 2014 – were used to calculate DOC flux at upstream and
460 downstream sites as $\text{flux}_{\text{DOCdown}} = [\text{DOC}]_{\text{down}} \bullet \text{discharge}_{\text{down}}$ or $\text{flux}_{\text{DOCup}} = [\text{DOC}]_{\text{up}} \bullet \text{discharge}_{\text{up}}$, and at
461 within-slump sites as $\text{flux}_{\text{DOCwithin}} = (\text{discharge}_{\text{down}} - \text{discharge}_{\text{up}})$. We calculate a similar mass balance for
462 TSS, which we use as a rough tracer for the inflow of slump runoff over the < 1 km span between
463 upstream and downstream locations at this site.

Formatted: Indent: First line: 0.5", No widow/orphan control

Deleted: ¶

465 4. Results

469 4.1 DOC concentration across slump sites

470 While DOC concentrations ranged broadly across pristine streams on the Peel Plateau (Fig. 2;
471 from 5.4 to 26.1 mg L⁻¹ at upstream, pristine sites), concentrations consistently declined downstream of
472 slumps, when compared to paired, upstream locations (p<0.001; Fig. 2; Table 2). Although this effect
473 was modest (typically less than 20%; Fig. 2), it occurred reliably across all slump sites. In contrast,
474 comparisons of upstream and within-slump sites showed no consistent trend in DOC concentration,
475 when evaluated across all slump locations (p=0.153; Fig. 2; Table 2). Instead, the effects of slumping on
476 the DOC concentration of slump runoff varied by site. At the largest, most well-developed slump
477 complexes (FM4, FM2, and FM3), where debris tongues are extensive and thaw extends well into the
478 deepest layer of Pleistocene-aged glacial materials, DOC concentrations tended to be lower in slump
479 runoff than at the paired upstream sites (Fig. 2). At more modestly-sized slump sites (HB, HC, and HD),
480 where the modern and relict Holocene active layers form a greater proportion of the actively thawing
481 headwall, within-slump DOC concentrations tended to be higher than values upstream (Fig. 2). Within
482 each site, DOC concentrations were relatively consistent across the 2-3 sampling periods (Fig. 2).
483

Deleted: On the Peel Plateau,

Formatted: Superscript

Deleted: was consistent

Deleted: appeared to vary

Deleted: However, there was significant variation in DOC concentration between slump locations (i.e., across the Peel Plateau landscape; Fig. 2).

484 4.2 Bulk chemistry of pristine waters and slump runoff

485 To better understand how the input of slump runoff affects downstream DOC, we examined
486 concentrations of major ions, conductivity and TSS as 'tracers' of slump activity, because these
487 constituents have previously been shown to be significantly affected by slumping in this region (Kokelj et
488 al., 2005, 2013; Malone et al., 2013; Thompson et al., 2008). Major ion (Ca²⁺, Mg²⁺, Na⁺) concentrations
489 in slump runoff were considerably greater than in pristine streams (a 2.7 to 11.7-fold increase; Fig. 3b-d;
490 Table 2). These patterns were similar, though muted, at slump-affected downstream sites, where major
491 ion concentrations were 1.5 to 3.5-fold greater than at pristine sites (Fig. 3b-d; Table 2). Average
492 conductivity also increased significantly as a result of slumping (p< 0.001; Table 2): within-slump sites
493 had conductivity values that were 9.2-fold greater than upstream sites, while downstream values were

Deleted: conservative

501 an average of 2.6 times greater than those upstream (Fig. 3e). Finally, TSS was also significantly elevated
502 at slump-affected sites ($p < 0.001$; Table 2) with levels being more than two orders of magnitude greater
503 within slumps when compared to upstream, and more than one order of magnitude greater
504 downstream, when compared to upstream sites (Fig. 3a). The effect of slump runoff on downstream
505 chemistry is also reflected in DOC: ion, and DOC: TSS ratios, which decreased markedly between
506 upstream and downstream locations. For example, molar ratios of $(Ca^{2+} + Mg^{2+})$: DOC averaged $0.78 \pm$
507 0.37 (mean \pm standard error) upstream of slumps, but 2.07 ± 0.45 downstream, while average gram-
508 weight ratios of TSS: DOC were 32 ± 12 upstream, but 1454 ± 332 at downstream locations.

509

510 *4.3 Spectral and isotopic characteristics*

511 SUVA₂₅₄, which is positively correlated with DOM aromaticity (Weishaar and Aiken, 2003), was
512 significantly lower within slumps, and downstream of slumps, than in upstream, pristine, environments
513 ($p < 0.001$; Fig. 4; Table 2). Average within-slump SUVA₂₅₄ was less than half of that observed for pristine
514 waters (Fig. 4), while downstream values declined by approximately 20%. In accordance with the
515 SUVA₂₅₄ results, $S_{275-295}$, $S_{350-400}$, and S_R were all significantly greater within slumps when compared to
516 upstream sites ($p < 0.001$; Fig. 4; Table 2), indicating lower DOM molecular weight within slumps (Helms
517 et al., 2008). Differences in slope parameters between upstream and downstream locations were muted
518 relative to the within-slump: upstream comparisons (Fig. 4), with $S_{275-295}$ ($p = 0.011$) and S_R ($p < 0.001$)
519 increasing significantly, but more modestly, downstream of slumps, and $S_{350-400}$ declining slightly
520 ($p = 0.001$; Fig. 4; Table 2).

521 Upstream $\delta^{18}O$ averaged $-20.1\text{‰} \pm 0.12$, which corresponds to a modern active layer pore water
522 $\delta^{18}O$ signature for this region (Lacelle et al., 2013; Fig. 5). Within-slump $\delta^{18}O$ was discernibly depleted
523 when compared to upstream locations, with average values of $-22.7\text{‰} \pm 0.72$, which falls between
524 previously-identified regional endmembers for Pleistocene-aged ground ice ($18,100 \pm 60$ ¹⁴Cyr BP) and
525 the modern active layer (Lacelle et al., 2013; Fig. 5). Within-slump $\delta^{18}O$ was also much more variable

526 between RTS features than upstream and downstream $\delta^{18}\text{O}$ values. Similar to upstream sites,
527 downstream $\delta^{18}\text{O}$ clustered near the modern active layer $\delta^{18}\text{O}$ endmember, but with a small depletion
528 that was consistent with a contribution from slump inflow ($-20.7\text{‰} \pm 0.21$).

529 To further investigate the effect of water source on DOM composition, we examined the
530 relationship between SUVA_{254} and $\delta^{18}\text{O}$. More depleted samples taken from within-slump sites had
531 clearly depressed SUVA_{254} values when compared to samples with more enriched $\delta^{18}\text{O}$ (Fig. 5). Of the
532 large, most well-developed slumps that were identified in Section 4.1, two (FM2 and FM3), in addition
533 to site HB, had $\delta^{18}\text{O}$ values that were more depleted than the Holocene-aged icy diamicton values
534 reported in Lacelle et al. (2013), suggesting some contribution of runoff from older, Pleistocene-aged
535 permafrost (Fig. 5). It is likely that the $\delta^{18}\text{O}$ signal at the relatively stable mega-slump site (FM4) was
536 somewhat diluted by the 7.2 mm of rainfall that fell in the 48 hours preceding our sample. Although
537 sites FM3 and SD received 12.4 and 3.5 mm of rain, respectively, in the 48 hours prior to sampling, these
538 are both much more active slump sites, and thus less prone to dilution of the slump outwash signature.
539 There was no significant rainfall immediately preceding sampling at any other sites.

540 The radiocarbon signature of DOC from upstream and within-slump locations at sites FM4, FM2,
541 FM3, and SD largely mirrors the $\delta^{18}\text{O}$ results. DOC from sites upstream of slump disturbances was
542 approximately modern in origin (ranging from 217 ± 24 ^{14}C yr BP to modern in age; Table 3). In contrast,
543 within-slump waters from site FM2 and FM3 were early Holocene-aged (9592 ± 64 , and 8167 ± 39 ^{14}C yr
544 BP, respectively; Table 3). Slump runoff from site SD was older than at upstream sites, but younger than
545 for the larger slumps, described above (1157 ± 23 ^{14}C yr BP; Table 3).

546

547 *4.4 Patterns and environmental drivers of DOC flux*

548 Similar to our findings for the distributed sampling scheme (Fig. 2), downstream DOC
549 concentration was consistently lower than concentrations upstream, across the 19 paired
550 measurements taken at the intensively studied slump site (slump FM3; $p < 0.001$, $N=19$, $W=0$; Wilcoxon

551 Signed Rank Test; mean decline of $2.5 \pm 0.2 \text{ mg L}^{-1}$, compared to a mean upstream concentration of 13.6
552 $\pm 0.5 \text{ mg L}^{-1}$. To explore environmental drivers of DOC movement within this landscape, however, we
553 focus on DOC flux, which allows a direct assessment of slump-mediated DOC addition to this system.
554 Downstream DOC flux (mg s^{-1}) tended to be slightly greater than upstream flux on most, but not all,
555 sampling occasions (Fig. 6). As a result, paired comparisons indicate no statistical difference between
556 upstream and downstream DOC flux at this site (Wilcoxon signed rank test; $p=0.096$, $N=19$, $W=53$).
557 Because upstream and downstream DOC flux were strongly correlated to one another ($r^2 = 0.94$;
558 $p<0.0001$), our downstream model was run without upstream DOC flux as a predictor variable. The best-
559 fit multiple linear regression model for downstream DOC flux ($r^2 = 0.84$; $p<0.01$) retained seven
560 variables, of which two were significant (Table 4). Of these, air temperature (72h prior to sampling)
561 showed a negative relationship with downstream DOC flux while rainfall (0h; time of sampling) showed
562 a strong positive relationship (Table 4). The best-fit model for upstream DOC flux ($r^2 = 0.87$; $p<0.001$)
563 also retained seven variables, of which four were significant ($p<0.05$; Table 4). Similar to the
564 downstream analysis, air temperature (0h, 72h) had a negative relationship, and time-of-sampling (0h)
565 rainfall had a strong positive relationship, with DOC flux (Table 4). However, 120h rainfall showed a
566 negative relationship with DOC flux in this model. Regressions assessing controls on downstream DOC
567 flux relative to upstream flux (i.e., as a ratio, or the difference between the two values) were not
568 significant. Models to explore controls on upstream and downstream DOC concentration were also
569 relatively similar to one another, showing strong, positive relationships between DOC concentration and
570 air temperature, and more modest negative relationships between DOC concentration and net radiation
571 (Table 4).

Deleted:)

Deleted: (as mg s^{-1})

Deleted: and

Deleted: exploring

Deleted: ing

579 **5. Discussion**

580 *5.1 Retrogressive thaw slumps and carbon delivery to streams of the Peel Plateau*

581 In both Eastern Siberia (Spencer et al. 2015; Vonk et al., 2013b) and Alaska (Abbott et al., 2014),
582 permafrost slumping has been associated with significant increases in DOC mobilization from
583 permafrost thaw features to aquatic systems. Our data show that this was not the case on the Peel
584 Plateau, where the landscape-induced variation in DOC concentration among pristine stream sites was
585 much greater than the change in stream water DOC as a result of slumping. Across all of our study sites,
586 DOC concentrations consistently decreased downstream of slumps when compared to upstream
587 locations, while at an intensively-sampled slump, DOC flux did not differ significantly between upstream
588 and downstream locations. In contrast, comparisons of channelized slump runoff (our within-slump
589 sites) and paired un-affected sites showed no consistent DOC trend. Instead, DOC concentrations in
590 slump runoff were either greater than, or less than, their comparison upstream locations, in a manner
591 that differed depending on slump morphological characteristics such as slump size and headwall height
592 (Fig. 1; see further discussion in Section 5.3). The moderate effect of slumping on DOC concentration
593 occurred despite the significant influence of these disturbances on the delivery of many biogeochemical
594 constituents to recipient streams. For example, conductivity was approximately one order of magnitude
595 greater, and TSS two orders of magnitude greater, in slump-derived runoff than at upstream, un-
596 affected sites. This led to substantially increased TSS:DOC and (Ca + Mg):DOC ratios downstream of
597 slumps, when compared to pristine, upstream locations.

598 Decreasing DOC concentrations downstream of slumps, despite increasing concentrations of
599 indicators of slump activity (major ions, TSS) could result from several, potentially co-occurring
600 mechanisms. In some locations, decreases may be partially caused by low DOC concentrations in slump
601 outflow (a dilution effect; see slumps FM2, FM3, and FM4 in Fig. 2; further discussed in Section 5.3).
602 However, our results suggest that DOC sorption to suspended inorganic sediments could also play a role
603 in regulating DOC dynamics in slump-affected systems on the Peel Plateau. At multiple sites (HB, HC, and

Deleted: (Drake et al., 2015; Mann et al., 2015; Vonk et al., 2013b),

Deleted: Balcarczyk et al., 2009;

Deleted: , and the Canadian High Arctic (Melville Island; Woods et al., 2011),

Deleted: to streams

Deleted: have

Deleted: causes

Deleted: ;

Deleted: field evidence suggests

614 HD), DOC concentrations declined downstream of slumps despite a modest elevation in DOC
 615 concentration in slump drainage waters (Fig. 2). Thermokarst contributes significant amounts of fine-
 616 grained glacial sediment to fluvial systems on the Peel Plateau (Kokelj et al., 2013; silty-clay sediment
 617 classification for FM3 in Lacelle et al., 2013). DOC sorption can occur in seconds to minutes in freshwater
 618 systems (Qualls and Haines, 1992), with fine-grained materials being particularly conducive to this
 619 process (Kothawala et al., 2009). Data from site FM3, where we have upstream and downstream
 620 discharge data coupled with DOC and TSS concentrations at upstream, downstream, and within-slump
 621 locations on two separate dates, allows us to assess possible DOC sorption at this site. On these dates,
 622 DOC flux declines downstream of the slump (i.e., $\text{flux}_{\text{DOCdown}} < \text{flux}_{\text{DOCup}}$), despite a clear and measurable
 623 efflux of DOC from the slump to the receiving stream system ($\text{flux}_{\text{DOCwithin}}$; Fig. 7). This same calculation
 624 using TSS as a rough tracer of slump inflow shows the calculated efflux of TSS from this slump
 625 ($\text{flux}_{\text{TSSwithin}}$) to be almost identical to the increase in TSS flux downstream of the disturbance (as
 626 $\text{flux}_{\text{TSSdown}} - \text{flux}_{\text{TSSup}}$; Fig. 7). Thus, it seems likely that relatively rapid processes, such as sorption to
 627 mineral surfaces, are affecting DOC dynamics in downstream fluvial systems on the Peel Plateau.

628 Although a similar decrease in DOC concentration with slumping has been found for lakes in this
 629 region (Kokelj et al., 2005), our findings contrast with work to-date in other areas of the Arctic, where
 630 thermokarst has been demonstrated to lead to an efflux of high-DOC waters from slump features (e.g.,
 631 Abbott et al., 2014; Vonk et al., 2013a). Ice-marginal glaciated landscapes are common throughout the
 632 western Canadian Arctic, however, and in many other Arctic regions. This terrain type is characterized by
 633 thick, mineral-rich but carbon-poor tills, and high ice contents that are predisposed to intense climate-
 634 driven thaw slumping and the release of glacial sediments (Kokelj et al., 2017b). As a result, DOC
 635 'sequestration' following slumping seems unlikely to be limited to the Peel Plateau. Given the high TSS
 636 export and apparent organic carbon sorption to glacial sediments observed with slumping on the
 637 Peel Plateau, we expect that substantial organic carbon is mobilized from these slumps in the particle-
 638 attached, rather than dissolved, form (i.e., as particulate organic carbon; POC). Quantifying this POC

- Deleted: (Kokelj et al., 2013), and this material is fine-grained
- Deleted: e.g., sediments from the FM3 headwall have been classified as silty clay;
- Deleted: these
- Deleted: es
- Deleted: within
- Deleted: calculated as $[\text{DOC}]_{\text{within}} \cdot (\text{discharge}_{\text{down}} - \text{discharge}_{\text{up}})$;
- Deleted: conservative
- Deleted: activity
- Deleted: within-slump flux
- Deleted: (as $[\text{TSS}]_{\text{within}} \cdot (\text{discharge}_{\text{down}} - \text{discharge}_{\text{up}})$)
- Deleted: difference
- Deleted: between
- Deleted: and upstream locations
- Deleted: is
- Deleted: of slumps
- Deleted: The
- Deleted: downstream of Peel Plateau slumps
- Deleted: is similar to, but more muted than results
- Deleted: ,
- Deleted: where following slump stabilization, lakes are characterized by increases in conductivity, clear decreases in DOC concentration, and a strong negative correlation between these two parameters
- Deleted: . The greater magnitude of effect for lakes in this region is likely caused by substantial particle settling in lentic environments, which enables DOC scavenging with the inorganic sediment inputs of thermokarst (Kokelj et al., 2005). Although decreasing DOC with RTS activity on the Peel Plateau
- Deleted: s
- Deleted: regions (e.g., Abbott et al., 2014; Vonk et al., 2013a),
- Deleted: i
- Deleted: intensely affected by RTS
- Deleted: ,
- Deleted: (Kokelj et al., 2017b). In general, t
- Deleted: typically
- Deleted:
- Deleted: which with their
- Deleted: Thus, it seems likely that
- Deleted: the processes we observe are not limited to the Peel Plateau: research to quantify

680 mobilization, its fate once subject to contemporary biogeochemical processing, and the mechanisms
681 that enable DOC sequestration to occur, are key avenues for future research, on the Peel Plateau and
682 elsewhere.

Deleted: via sorption processes seems warranted across regions where thermokarst intensifies the transport of mineral-rich sediments to downslope aquatic systems.

684 5.2 The effect of retrogressive thaw slumps on DOM composition

685 Despite the fact that DOC concentrations did not increase in RTS-affected streams, absorbance
686 metrics clearly indicate that slump-derived DOM on the Peel Plateau is compositionally different than
687 DOM from upstream locations. Upstream waters had significantly higher SUVA₂₅₄ values than
688 downstream and within-slump sites (Table 2, Fig. 4). Similarly, while the average S_R of Peel Plateau
689 upstream waters (0.74 ± 0.005) was within the range of S_R typically associated with fresh, terrestrial
690 DOM (~ 0.70; Helms et al., 2008), values were significantly greater within-slump (0.92 ± 0.015) and
691 downstream (0.89 ± 0.009) (Table 2, Fig. 4), indicating decreasing DOM molecular weight as a result of
692 RTS activity. High SUVA₂₅₄ values accompanied by low S_R at upstream sites suggest that water flow in
693 undisturbed catchments is restricted to shallow, organic-rich flowpaths through the active layer, with
694 permafrost inhibiting water contributions from deeper, groundwater or mineral-associated sources
695 (Balcarczyk et al., 2009; MacLean et al., 1999; Mann et al., 2012; O'Donnell et al., 2010; Street et al.
696 2016). In contrast, within-slump and downstream measurements indicate a clear transition in DOM
697 source.

Deleted: , SUVA₂₅₄ and

Deleted: compared to

698 The comparatively low SUVA₂₅₄, and high S_R values for downstream and within-slump sites
699 indicate that permafrost-derived carbon on the Peel Plateau is characterized by relatively low molecular
700 weight and aromaticity, and is thus similar in its composition to permafrost carbon from other regions.
701 For example, SUVA₂₅₄ values were low in waters draining active thaw slumps when compared to
702 stabilized and undisturbed sites on the North Slope of Alaska (Abbott et al., 2014), while in Siberia, ¹⁴C-
703 depleted DOM from small tributary streams affected by thermokarst had lower SUVA₂₅₄ values
704 compared to younger DOM from the Kolyma River mainstem (Mann et al., 2015; Neff et al., 2006).

710 Although SUVA₂₅₄ values for waters draining Peel Plateau thaw slumps are slightly lower than those
711 reported for Siberian Yedoma disturbances (Mann et al., 2015), the overall similarity of permafrost-
712 derived DOM composition across these various regions is striking, given the regional differences in
713 permafrost origin and depositional history. For example, while the DOM released by permafrost thaw on
714 the Peel Plateau is till-associated, and early-Holocene in mean age, east Siberian Yedoma is composed of
715 loess-derived Pleistocene deposits that sequestered carbon in association with synnetic aggradation
716 of permafrost. This suggests that common processes may enable the organic matter contained in
717 permafrost soils to become compositionally similar across diverse Arctic regions. Such compositional
718 similarity also indicates that permafrost-origin DOM from the Peel Plateau – similar to that from other
719 regions (Abbott et al., 2014; Drake et al., 2015) – may be readily degraded by bacteria, despite the
720 divergent origin of this carbon.

721

722 5.3 The effect of slump morphometry on runoff water biogeochemistry

723 $\delta^{18}\text{O}$ and DO^{14}C data provide further evidence that intense slumping enables novel sources of
724 water and solutes to be transported to fluvial systems on the Peel Plateau. For most of the RTS features
725 that we studied, the $\delta^{18}\text{O}$ signature of within-slump waters ranged from those similar to the ‘icy
726 diamicton’ that overlies the early Holocene thaw unconformity, to those for underlying Pleistocene-aged
727 ground ice (Lacelle et al., 2013; Fig. 5). Similarly, DO^{14}C from a subset of sites indicates slump-derived
728 DOC is early Holocene in age for all but the shallowest slump surveyed. This suggests that our slump
729 outflow samples were likely comprised of a mixture of Pleistocene-, Holocene-, and modern-sourced
730 water (see Fig. 1c-e), but that the contribution of these end-members varied across slumps depending
731 on the relative volume of different stratigraphic units being mobilized.

732 The between-site variation in $\delta^{18}\text{O}$ signature (Fig. 5) and relative DOC concentration (Fig. 2b) of
733 slump runoff waters appears to be related to differences in slump morphometry (size, headwall height,
734 and the length and area of the debris tongue; see Table 1 and Fig. 1c-e) across sites. The well-developed,

Deleted: -aged

736 larger slump complexes (FM4, FM2 and FM3) were more likely to have $\delta^{18}\text{O}$ signatures that lie between
737 end-member values for Holocene-aged icy diamicton and Pleistocene-aged ground ice (Fig. 5; although
738 note that dry and stabilized FM4 differs somewhat from this trend). These well-developed slumps also
739 stood out as displaying within-slump DOC concentrations that were lower than at upstream comparison
740 sites (Fig. 2b). The headwall exposure at these largest slumps exposes Pleistocene-aged permafrost to
741 several metres depth (see Fig. 1c), while the evacuation of scar zone materials have produced extensive
742 debris tongues up to several kilometers long (Table 1, Figs. 1b, S1e and S1g). This significant exposure of
743 mineral-rich, Pleistocene-aged glacial till contributes solutes from low-carbon mineral soils and low-DOC
744 ground ice (Fritz et al. 2015; Tanskii et al. 2016) to runoff, while entraining fine-grained sediments which
745 provide mineral surface area for possible DOC adsorption. Adsorption may be further enhanced as
746 slump and stream runoff continue to entrain sediments as flows incise the lengthy debris tongue
747 deposits. In contrast, slumps with slightly shallower headwalls (HA, HB, HC, HD; see Fig. 1d), and less
748 well-developed debris tongues (Table 1), appear to elicit a slightly different response than the largest
749 slumps discussed above. At these mid-sized sites, within-slump DOC concentrations were typically
750 higher than those found at upstream comparison sites (Fig. 2b), which may reflect the greater relative
751 inputs from thawing of the Holocene-aged relict active layer, and decreased interaction with debris
752 tongue deposits at these smaller disturbances. Similarly, runoff $\delta^{18}\text{O}$ tends to lie between Holocene and
753 modern end-member values at these sites (though note the more depleted value for HB; Fig. 5),
754 indicating a lower relative contribution of Pleistocene-aged ground ice to slump outflow waters.

755 Finally, the youngest and shallowest slump surveyed (SD), exposes only near-surface permafrost
756 soils for leaching and geochemical transport (Figs. 1e and S1; Table 1), and not the underlying mineral
757 and ice-rich glacial substrates. Accordingly, the effects of slumping on stream chemistry, optical
758 parameters, and isotopes appear muted at SD when compared to the larger slumps discussed above.
759 These morphometry-related shifts in the downstream effects of slumping suggest that we should expect
760 non-linearity in the biogeochemical response as RTS features develop over time, particularly if slumping

Deleted: slump

762 continues to intensify with future warming on the Peel Plateau (e.g., Kokelj et al., 2017b). This
763 underscores the importance of long-term monitoring on the Peel Plateau and elsewhere, and indicates
764 that the incorporation of non-linearity into modelling efforts is critical for predicting future change,

Deleted: L

Deleted: models

Deleted: , are clearly warranted for the Peel Plateau and elsewhere in the Arctic

766 5.4 Environmental controls on DOC flux and concentration

767 Air temperature and rainfall exerted the strongest control on DOC flux at our intensively studied
768 site, which was chosen to be representative of active Peel Plateau slumps that are eroding Holocene- to
769 Pleistocene-aged sediments (slump FM3; Fig. 6; Table 4). Upstream of the slump, rainfall was positively
770 correlated, and air temperature negatively correlated, with DOC flux. However, precipitation events are
771 negatively related to temperature at the upstream site (Fig. 6), suggesting that at the single-season scale
772 of our investigation, precipitation served as the primary environmental control on DOC flux. DOC

Deleted:

Deleted: this

773 concentration was relatively constant with discharge upstream ($r=-0.342$, $p=0.151$), indicating that
774 precipitation controls DOC flux largely as a result of changes in water flow in pristine streams on the
775 Peel Plateau, and that DOC was not source-limited over the time scale of our investigation. However,
776 upstream DOC concentration was positively related to temperature (Table 4), suggesting that biological

Deleted: at the

Deleted: site

Deleted: at this site

Deleted: source

Deleted: , however

777 activity is an important regulator of within-soil DOC production (c.f. Pumpanen et al., 2014). These
778 upstream-of-slump results are consistent with work from other undisturbed permafrost and boreal
779 regions, where precipitation and catchment runoff have been shown to control DOC flux in streams
780 (Prokushkin et al., 2005; Pumpanen et al., 2014), and increasing temperature has been shown to
781 increase DOC production in soils (Christ and David, 1996; Neff and Hooper, 2002; Prokushkin et al.,
782 2005; Yanagihara et al., 2000). They are also consistent with the concept that the permafrost barrier
783 forces precipitation to travel through the shallow active layer, where high hydraulic conductivity leads to
784 rapid transport of carbon into fluvial systems, and little degradation in soils (O'Donnell et al., 2010;
785 Striegl et al., 2005).

Deleted: impermeable

Deleted:

799 Slumping did not significantly affect downstream DOC flux at the intensively studied slump site,
 800 when compared to DOC flux upstream of this site (Fig. 6; Section 4.4). Although concentration
 801 consistently declined downstream at FM3 (Sections 4.1 and 4.4), downstream DOC flux was either
 802 slightly higher, or slightly lower, than upstream flux; a result that seems likely to play out at other,
 803 comparable Peel Plateau slumps, given the coherent concentration patterns that we observed with
 804 slumping. Concordant with the lack of change in DOC flux in response to slumping, neither the ratio of
 805 (downstream: upstream) or difference between (downstream – upstream) upstream and downstream
 806 DOC flux could be explained by any of our environmental variables, while downstream flux showed an
 807 almost identical relationship with environmental controls as those upstream (Table 4). The lack of clear
 808 environmental control on relative downstream: upstream DOC flux occurred despite the fact that
 809 precipitation has been shown to be a strong driver of ablation and sediment movement from slump
 810 features on the Peel Plateau, at time scales similar to those used for this work (Kokelj et al., 2015).

811 Considering the Peel Plateau landscape as a whole, it appears that precipitation serves as a
 812 primary, positive control on DOC flux. Thus, this study adds DOC production to the list of changes – such
 813 as increasing slump activity and sediment mobilization – that can be expected with the increases in
 814 precipitation that are underway in this region, and are predicted for many Arctic regions (IPCC, 2014;
 815 Kokelj et al., 2015). However, it appears that slumping does not over-ride the landscape-scale control on
 816 DOC flux in this system – at least at the scale of this single-season – perhaps because processes like DOC
 817 sorption mask the influx of slump-derived DOC (Fig. 6). This result highlights the complexity of the
 818 interaction between changing climatic parameters and DOC dynamics on the Peel Plateau, where slump
 819 features of increasing size incorporate thawing till, glaciolacustrine, glaciofluvial, and organic deposits,
 820 while also draining contemporary active layers across a shrub-tundra to spruce forest upland gradient,
 821 DOC dynamics are thus affected by both water and carbon generation across these variable landform
 822 types, and by biogeochemical interactions such as mineral adsorption in recipient systems. While future
 823 work to tease apart the interactions between changing climatic parameters, slump development, and

Deleted: modify

Deleted: slump FM3

Deleted: this site

Deleted: values

Deleted: , across the multiple measurement points

Deleted: that we considered

Deleted: this

Deleted: finding

Deleted: expected throughout the Arctic

Deleted: ; Walsh et al., 2011

Deleted: clearly

Deleted: ;

Deleted: additionally

Deleted: ;

Deleted: and where

Deleted: variably

Deleted: It also underscores the need for

841 resultant biogeochemical effects is clearly warranted on the Peel Plateau and elsewhere, we must also
842 recognize that environmental controls on slump activity and thus downstream biogeochemistry can be
843 expected to show marked regional variation (see for example, work from Eureka Sound; Grom & Pollard
844 2008).

Deleted: ; both

Deleted: across the Arctic

Deleted: where

846 5.5 Study implications and future research directions: Dissolved carbon mobilization across diverse
847 permafrost landscapes

Deleted: dissolved

848 Carbon dynamics in Arctic aquatic systems are influenced by numerous factors, including
849 geology, Quaternary and glacial history, soil composition, vegetation, active layer dynamics, and the
850 nature and intensity of thermokarst. As a result, the effect of permafrost thaw on DOC concentration

851 and flux should – at a fundamental level – vary across broad, regional scales. Our results demonstrate,

Deleted: This study

852 that we can expect marked inter-regional variation in DOC transport to streams in response to

Deleted: s

Deleted: large

853 permafrost degradation. For example, declines in DOC concentration downstream of slumps on the Peel

Deleted: s

Deleted: , and that results from multiple regions are needed to understand change across the Arctic as whole

854 Plateau clearly differ from what has been found in eastern Siberia and regions of Alaska, where

Deleted: The

855 thermokarst releases substantial quantities of DOC (e.g., Spencer et al. 2015), and increases DOC

Deleted: strikingly

856 concentrations in downstream systems (Abbott et al. 2015). Efforts that incorporate information

Deleted: for example,

Deleted: significantly

857 concerning the geology and Quaternary history of thawing landscapes, the physical and geochemical

Deleted: Modelling e

Deleted: that are being thawed

858 composition of permafrost soils, and the nature and intensity of thermokarst processes within

Deleted: the

859 landscapes (see, for example, Olefeldt et al. 2016) will considerably increase our ability to accurately

Deleted: would

Deleted: clearly enable more accurate predictions

860 predict how carbon delivery from land to water will respond to climate change on a pan-Arctic scale.

Deleted: of

861 At finer scales, however, this work underscores the variability of thermokarst effects within

Deleted: underlines

862 regions, and the local-scale control on this variability. On the Peel Plateau, for example, between-site

863 differences in the biogeochemical effect of thermokarst correspond to variation in soil stratigraphy (i.e.,

Deleted: s

864 the relative depth of the Holocene aged paleo-active layer) and ever-evolving slump morphometry.

865 Although striking within-region variability in biogeochemical response to thermokarst has been seen

Deleted: the

Deleted: effects of

890 elsewhere (e.g., Watanabe et al., 2011), responses in other regions occur as a result of very different –
891 and region-specific – landscape-level drivers. This landscape-specificity also extends to the non-linear,
892 biogeochemical response as slump features develop over time. Changes in downstream
893 biogeochemistry with slump development are very different on the Peel Plateau, for example, than in
894 other regions (e.g., Abbot et al. 2015), while non-linearity can also be expected to extend to different
895 types of permafrost thaw (Kokelj et al. 2002, Vonk et al. 2016), such as increasing active layer thickness
896 (Romanovsky et al. 2010). Only with a tiered approach, where we work within regions to understand
897 how local controls drive regional responses to thaw, and across regions to document how predictable,
898 broad-scale variation controls responses at continental to pan-Arctic scales, will we be able to
899 understand the future biogeochemical functioning of thermokarst-affected landscapes throughout
900 Arctic regions.

Deleted: it

Deleted: s

Deleted: ity of

Deleted: the

Deleted: The changing response of

Deleted: is

Deleted: focus

Deleted: and changing effects over time

Deleted: affects the nature of thermokarst effects

Deleted: truly

Deleted: at the pan-Arctic scale

901

902

903 Acknowledgements

904 Financial support for this research was provided by Ontario Graduate Scholarship, York University
905 Fieldwork Cost Fund, York University Research Cost Fund, Northern Scientific Training Program, NSERC
906 Discovery and Northern Research Supplement grants to SET, the Campus Alberta Innovates Program,
907 and the Polar Continental Shelf Program. We would like to thank Scott Zolkos for his support as a field
908 assistant and for the production of Figure 1; S. Tetlich, D. Neyando, and P. Snowshoe for field sampling
909 assistance; and the Tetlit Gwich'in (Fort McPherson) Renewable Resources Council. Sarah Shakil and
910 Scott Zolkos assisted with the collection of samples for DO¹⁴C; Justin Kokoszka performed geospatial
911 calculations of slump area and debris tongue length. Comments from Michael Fritz and one anonymous
912 reviewer greatly improved the content of the manuscript.

924 **Literature Cited**

- 925 Abbott, B. W., Larouche, J. R., Jones, J. B., Bowden, W. B., and Balsler, A. W.: Elevated dissolved organic
926 carbon biodegradability from thawing and collapsing permafrost, *J. Geophys. Res.*, 119, 2049–2063,
927 doi:10.1002/2014JG002678, 2014.
- 928 Abbott, B. W., Jones, J. B., Godsey, S. E., Larouche, J. R., and Bowden, W. B.: Patterns and persistence of
929 hydrologic carbon and nutrient export from collapsing upland permafrost, *Biogeosciences*, 12, 3725–
930 3740, doi:10.5194/bg-12-3725-2015, 2015.
- 931 Balcarczyk, K. L., Jones, J. B., Jaffé, R., and Maie, N.: Stream dissolved organic matter bioavailability and
932 composition in watersheds underlain with discontinuous permafrost, *Biogeochemistry*, 94, 255–270,
933 doi:10.1007/s10533-009-9324-x, 2009.
- 934 Battin, T. J., Kaplan, L. A., Findlay, S., Hopkinson, C. S., Marti, E., Packman, A. I., Newbold, J. D., and
935 Sabater, F.: Biophysical controls on organic carbon fluxes in fluvial networks, *Nat. Geosci.*, 1, 95–100,
936 doi:10.1038/ngeo101, 2008.
- 937 Burn, C. R.: Cryostratigraphy, paleogeography, and climate change during the early Holocene warm
938 interval, western Arctic coast, Canada. *Can. J. Earth Sci.* 34, 912-925, doi: 10.1139/e17-076, 1997.
- 939 Burn, C. R. and Kokelj, S. V.: The environment and permafrost of the Mackenzie Delta area, *Permafrost
940 Periglac. Process.*, 20, 83–105, doi:10.1002/ppp.655, 2009.
- 941 Burnham, K. P. and Anderson, D. R.: *Model Selection and Multi- Model Inference: A Practical
942 Information-Theoretic Approach*, Springer, New York., 2002.
- 943 Chin, K. S., Lento, J., Culp, J. M., Lacelle, D., and Kokelj, S. V.: Permafrost thaw and intense thermokarst
944 activity decreases abundance of stream benthic macroinvertebrates, *Glob. Chang. Biol.*, 22, 2715–2728,
945 doi:10.1111/gcb.13225, 2016.
- 946 Christ, M. J. and David, M. B.: Temperature and moisture effects on the production of dissolved organic
947 carbon in a Spodosol, *Soil Biol. Biochem.*, 28, 1191–1199, doi:10.1016/0038-0717(96)00120-4, 1996.
- 948 Curtin, J.: *lmSupport: Support for Linear Models*. R package version 2.9.2., 2015.
- 949 Dittmar, T. and Kattner, G.: The biogeochemistry of the river and shelf ecosystem of the Arctic Ocean: a
950 review, *Mar. Chem.*, 83, 103–120, doi:10.1016/S0304-4203(03)00105-1, 2003.
- 951 Drake, T. W., Wickland, K. P., Spencer, R. G. M., McKnight, D. M., and Striegl, R. G.: Ancient low-
952 molecular-weight organic acids in permafrost fuel rapid carbon dioxide production upon thaw, *Proc.
953 Natl. Acad. Sci.*, 112, 13946–13951, doi:10.1073/pnas.1511705112, 2015.
- 954 Duk-Rodkin, A. and Hughes, O. L.: *Surficial Geology, Fort McPherson-Bell River, Yukon-Northwest
955 Territories*. Geological Survey of Canada, Map 1745A, scale 1:250 000, Geological Survey of Canada, Map
956 1745A, scale 1:250 000, 1992.
- 957 Durbin, J. and Watson, G. S.: Testing for serial correlation in least squares regression I, *Biometrika*, 37,
958 409–428, 1950.
- 959 Environment Canada: *Canadian Climate Normals 1981-2010 Station Data, Fort McPherson*, 2015.
- 960 Fox, J. and Weisberg, S.: *An {R} Companion to Applied Regression, Second Edition*. Thousand Oaks CA:

Field Code Changed

Deleted: Catto, N. R.: Richardson Mountains, Yukon-Northwest Territories: The northern portal of the postulated "Ice-Free Corridor," *Quat. Int.*, 32, 3–19, doi:10.1016/1040-6182(95)00062-3, 1996.¶

- 965 Sage. <http://socserv.socsci.mcmaster.ca/jfox/Books/Companion.>, 2011.
- 966 Frey, K. E. and McClelland, J. W.: Impacts of permafrost degradation on arctic river biogeochemistry,
967 *Hydrol. Process.*, 23, 169–182, doi:10.1002/hyp, 2009.
- 968 Fritz, M., Vonk, J. E., and Lantuit, H.: Disappearing Arctic coastlines, *Nat. Clim. Change*, 7, 6-7,
969 doi:10.1038/nclimate3188, 2017.
- 970 Fritz, M., Opel, T., Tanski, G., Herzsuh, U., Meyer, H., Eulenburg, A., and Lantuit, H.: Dissolved organic
971 carbon (DOC) in Arctic ground ice, *The Cryosphere*, 9, 737-752, doi:10.5194/tc-9-737-2015, 2015.
- 972 Fritz, M., Wetterich, S., Schirrmeister, L., Meyer, H., Lantuit, H., Preusser, F., and Pollard, W. H.: Eastern
973 Beringia and beyond: Late Wisconsinan and Holocene landscape dynamics along the Yukon Coastal
974 Plain, Canada. *Palaeogeogr. Palaeoclimatol. Palaeoecol.*, 319–320, 28–45, doi:
975 10.1016/j.palaeo.2011.12.015, 2012.
- 976 Fulton, R. J.: *Surficial Materials of Canada*, Natural Resources Canada., 1995.
- 977 Green, S. A. and Blough, N. V.: Optical absorption and fluorescence properties of chromophoric
978 dissolved organic matter in natural waters, *Limnol. Oceanogr.*, 39, 1903–1916,
979 doi:10.4319/lo.1994.39.8.1903, 1994.
- 980 Hair, J. F. J., Anderson, R. E., Tatham, R. L., and Black, W. C.: *Multivariate Data Analysis*, 3rd ed.,
981 Macmillan, New York., 1995.
- 982 Hedges, J. I., Keil, R. G., and Benner, R.: What happens to terrestrial organic matter in the ocean?, *Org.*
983 *Geochem.*, 27, 195–212, 1997.
- 984 Helms, J. R., Stubbins, A., Ritchie, J. D., Minor, E. C., Kieber, D. J., and Mopper, K.: Absorption spectral
985 slopes and slope ratios as indicators of molecular weight, source, and photobleaching of chromophoric
986 dissolved organic matter, *Limnol. Oceanogr.*, 53, 955–969, doi:10.4319/lo.2008.53.3.0955, 2008.
- 987 Holmes, R. M., McClelland, J. W., Peterson, B. J., Tank, S. E., Bulygina, E., Eglinton, T. I., Gordeev, V. V.,
988 Gurtovaya, T. Y., Raymond, P. A., Repeta, D. J., Staples, R., Striegl, R. G., Zhulidov, A. V., and Zimov, S. A.:
989 Seasonal and annual fluxes of nutrients and organic matter from large rivers to the Arctic Ocean and
990 surrounding seas, *Estuaries and Coasts*, 35, 369–382, doi:10.1007/s12237-011-9386-6, 2012.
- 991 Hugelius, G., Strauss, J., Zubrzycki, S., Harden, J. W., Schuur, E. A. G., Ping, C. L., Schirrmeister, L., Grosse,
992 G., Michaelson, G. J., Koven, C. D., O'Donnell, J. A., Elberling, B., Mishra, U., Camill, P., Yu, Z., Palmtag, J.,
993 and Kuhry, P.: Estimated stocks of circumpolar permafrost carbon with quantified uncertainty ranges
994 and identified data gaps, *Biogeosciences*, 11, 6573–6593, doi:10.5194/bg-11-6573-2014, 2014.
- 995 IPCC: Topic 2: Future Climate Changes, Risks, and Impacts *In* *Climate Change 2014: Synthesis Report.*
996 *Contribution of Working Groups I, II and III to the Fifth Assessment Report of the Intergovernmental*
997 *Panel on Climate Change [Core Writing Team, R.K. Pachauri and L.A. Meyer (eds.)]. IPCC, Geneva,*
998 *Switzerland, 151 pp, Geneva, Switzerland., 2014.*
- 999 Kaiser, K. and Guggenberger, G.: The role of DOM sorption to mineral surfaces in the preservation of
1000 organic matter in soils, *Org. Geochem.*, 31, 711–725, doi:10.1016/S0146-6380(00)00046-2, 2000.
- 1001 Khvorostyanov, D. V., Krinner, G., Ciais, P., Heimann, M., and Zimov, S. A.: Vulnerability of permafrost
1002 carbon to global warming. Part I: Model description and role of heat generated by organic matter

- 1003 decomposition, *Tellus, Ser. B Chem. Phys. Meteorol.*, 60 B, 250–264, doi:10.1111/j.1600-
1004 0889.2007.00333.x, 2008a.
- 1005 Khvorostyanov, D. V., Ciais, P., Krinner, G., Zimov, S. A., Corradi, C., and Guggenberger, G.: Vulnerability
1006 of permafrost carbon to global warming. Part II: Sensitivity of permafrost carbon stock to global
1007 warming, *Tellus, Ser. B Chem. Phys. Meteorol.*, 60 B, 265–275, doi:10.1111/j.1600-0889.2007.00336.x,
1008 2008b.
- 1009 Kokelj, S. V, Tunnicliffe, J. F., and Lacelle, D.: The Peel Plateau of northwestern Canada : an ice-rich
1010 hummocky moraine landscape in transition, in *Landscapes and Landforms of western Canada*, edited by
1011 O. Slaymaker, pp. 109–122, Springer International Publishing, Switzerland., 2017a.
- 1012 Kokelj, S. V. and Jorgenson, M. T.: Advances in thermokarst research, *Permafr. Periglac. Process.*, 24,
1013 108–119, doi:10.1002/ppp.1779, 2013.
- 1014 Kokelj, S. V., Smith, C. A., and Burn, C. R.: Physical and chemical characteristics of the active layer and
1015 permafrost, Herschel Island, western Arctic Coast, Canada, *Permafr. Periglac. Process.*, 13, 171–185,
1016 doi:10.1002/ppp.417, 2002.
- 1017 Kokelj, S. V., Jenkins, R. E., Milburn, D., Burn, C. R., and Snow, N.: The influence of thermokarst
1018 disturbance on the water quality of small upland lakes, Mackenzie Delta region, Northwest Territories,
1019 Canada, *Permafr. Periglac. Process.*, 16, 343–353, doi:10.1002/ppp.536, 2005.
- 1020 Kokelj, S. V., Lantz, T. C., Kanigan, J. C., Smith, S. L., and Coutts, R.: Origin and polycyclic behaviour of
1021 tundra thaw slumps, Mackenzie Delta region, Northwest Territories, Canada, *Permafr. Periglac. Process.*,
1022 20, 173–184, doi:10.1002/ppp, 2009.
- 1023 Kokelj, S. V., Lacelle, D., Lantz, T. C., Tunnicliffe, J., Malone, L., Clark, I. D., and Chin, K. S.: Thawing of
1024 massive ground ice in mega slumps drives increases in stream sediment and solute flux across a range of
1025 watershed scales, *J. Geophys. Res. Earth Surf.*, 118, 681–692, doi:10.1002/jgrf.20063, 2013.
- 1026 Kokelj, S. V., Tunnicliffe, J., Lacelle, D., Lantz, T. C., Chin, K. S., and Fraser, R.: Increased precipitation
1027 drives mega slump development and destabilization of ice-rich permafrost terrain, northwestern
1028 Canada, *Glob. Planet. Change*, 129, 56–68, doi:10.1016/j.gloplacha.2015.02.008, 2015.
- 1029 Kokelj, S. V., Lantz, T. C., Tunnicliffe, J., Segal, R., and Lacelle, D.: Climate-driven thaw of permafrost
1030 preserved glacial landscapes, northwestern Canada, *Geology*, 45, 371–374, doi:10.1130/G38626.1,
1031 2017b.
- 1032 Kothawala, D. N., Moore, T. R., and Hendershot, W. H.: Soil properties controlling the adsorption of
1033 dissolved organic carbon to mineral soils, *Soil Sci. Soc. Am. J.*, 73, 1831–1842,
1034 doi:10.2136/sssaj2008.0254, 2009.
- 1035 Lacelle, D., Bjornson, J., and Lauriol, B.: Climatic and geomorphic factors affecting contemporary (1950-
1036 2004) activity of retrogressive thaw slumps on the Aklavik Plateau, Richardson Mountains, NWT,
1037 Canada, *Permafr. Periglac. Process.*, 21, 1–15, doi:10.1002/ppp.666, 2010.
- 1038 Lacelle, D., Lauriol, B., Zazula, G., Ghaleb, B., Utting, N., and Clark, I. D.: Timing of advance and basal
1039 condition of the Laurentide Ice Sheet during the last glacial maximum in the Richardson Mountains,
1040 NWT, *Quat. Res. (United States)*, 80, 274–283, doi:10.1016/j.yqres.2013.06.001, 2013.
- 1041 Lacelle, D., Fontaine, M., Forest, A. P., and Kokelj, S.: High-resolution stable water isotopes as tracers of

1042 thaw unconformities in permafrost: A case study from western Arctic Canada, *Chem. Geol.*, 368, 85–96,
1043 doi:10.1016/j.chemgeo.2014.01.005, 2014.

1044 Lacelle, D., Brooker, A., Fraser, R. H., and Kokelj, S. V.: Distribution and growth of thaw slumps in the
1045 Richardson Mountains–Peel Plateau region, northwestern Canada, *Geomorphology*, 235, 40–51,
1046 doi:10.1016/j.geomorph.2015.01.024, 2015.

1047 Lafrenière, M. J. and Lamoureux, S. F.: Thermal perturbation and rainfall runoff have greater impact on
1048 seasonal solute loads than physical disturbance of the active layer, *Permafrost Periglacial Process.*, 24, 241–
1049 251, doi:10.1002/ppp.1784, 2013.

1050 Lang, S. Q., McIntyre, C. P., Bernasconi, S. M., Früh-Green, G. L., Voss, B. M., Eglinton, T. I., and Wacker,
1051 L.: Rapid ¹⁴C analysis of dissolved organic carbon in non-saline waters, *Radiocarbon*, 58, 505–515,
1052 doi:10.1017/RDC.2016.17, 2016.

1053 Lantuit, H. and Pollard, W. H.: Fifty years of coastal erosion and retrogressive thaw slump activity on
1054 Herschel Island, southern Beaufort Sea, Yukon Territory, Canada, *Geomorphology*, 95, 84–102,
1055 doi:10.1016/j.geomorph.2006.07.040, 2008.

1056 Lantuit, H., Pollard, W. H., Couture, N., Fritz, M., Schirrmeister, L., Meyer, H., and Hubberten, H.W.:
1057 Modern and late Holocene retrogressive thaw slump activity on the Yukon Coastal Plain and Herschel
1058 Island, Yukon Territory, Canada. *Permafrost Periglacial Process.* 23, 39–51, doi: 10.1002/ppp.1731, 2012.

1059 Lantz, T. C. and Kokelj, S. V.: Increasing rates of retrogressive thaw slump activity in the Mackenzie Delta
1060 region, N.W.T., Canada, *Geophys. Res. Lett.*, 35, 1–5, doi:10.1029/2007GL032433, 2008.

1061 Lewkowicz, A. G.: Rate of short-term ablation of exposed ground ice, Banks Island, Northwest
1062 Territories, Canada, *J. Glaciol.*, 32, 511–519, 1986.

1063 Lewkowicz, A. G.: Headwall retreat of ground-ice slumps, Banks Island, Northwest Territories, *Can. J.*
1064 *Earth Sci.*, 24, 1077–1085, doi:10.1139/e87-105, 1987.

1065 MacLean, R., Oswood, M. W., Irons, J. G., and McDowell, W. H.: The effect of permafrost on stream
1066 biogeochemistry: A case study of two streams in the Alaskan (U.S.A.) taiga, *Biogeochemistry*, 47, 239–
1067 267, doi:10.1007/BF00992909, 1999.

1068 Malone, L., Lacelle, D., Kokelj, S., and Clark, I. D.: Impacts of hillslope thaw slumps on the geochemistry
1069 of permafrost catchments (Stony Creek watershed, NWT, Canada), *Chem. Geol.*, 356, 38–49,
1070 doi:10.1016/j.chemgeo.2013.07.010, 2013.

1071 Manley, W. F. and Kaufman, D. S.: *Alaska Paleoglacier Atlas*: Institute of Arctic and Alpine Research
1072 (INSTAAR), University of Colorado., 2002.

1073 Mann, P. J., Davydova, A., Zimov, N., Spencer, R. G. M., Davydov, S., Bulygina, E., Zimov, S., and Holmes,
1074 R. M.: Controls on the composition and lability of dissolved organic matter in Siberia’s Kolyma River
1075 basin, *J. Geophys. Res. Biogeosciences*, 117, G01028, doi:10.1029/2011JG001798, 2012.

1076 Mann, P. J., Eglinton, T. I., McIntyre, C. P., Zimov, N., Davydova, A., Vonk, J. E., Holmes, R. M., and
1077 Spencer, R. G. M.: Utilization of ancient permafrost carbon in headwaters of Arctic fluvial networks, *Nat.*
1078 *Commun.*, 6, 7856, doi: 10.1038/ncomms8856, 2015.

1079 McDowell, W. H.: Kinetics and mechanisms of dissolved organic carbon retention in a headwater stream,

1080 Biogeochemistry, 1, 329–352, 1985.

1081 Murton, J. and French, H.: Cryostructures in permafrost, Tuktoyaktuk coastlands, western arctic Canada,
 1082 Can. J. Earth Sci., 31, 737–747, doi:10.1139/e94-067, 1994.

1083 Murton, J. B., Edwards, M. E., Lozhkin, A. V., Anderson, P. M., Savvinov, G. N., Bakulina, N., Bondarenko,
 1084 O. V., Cherepanova, M. V., Danilov, P. P., Boeskorov, V., Goslar, T., Grigoriev, S., Gubin, S. V., Korzun, J. A.,
 1085 Lupachev, A. V., Tikhonov, A., Tsygankova, V. I., Vasilieva, G. V., and Zanina, O. G.: Preliminary
 1086 paleoenvironmental analysis of permafrost deposits at Batagaika megaslump, Yana Uplands, northeast
 1087 Siberia, *Quat. Res.*, 87, 314–330, doi:10.1017/qua.2016.15, 2017.

1088 Neff, J. C. and Hooper, D. U.: Vegetation and climate controls on potential CO₂, DOC and DON
 1089 production in northern latitude soils, *Glob. Chang. Biol.*, 8, 872–884, doi:10.1046/j.1365-
 1090 2486.2002.00517.x, 2002.

1091 Neff, J. C., Finlay, J. C., Zimov, S. A., Davydov, S. P., Carrasco, J. J., Schuur, E. A. G., and Davydova, A. I.:
 1092 Seasonal changes in the age and structure of dissolved organic carbon in Siberian rivers and streams,
 1093 *Geophys. Res. Lett.*, 33, 1–5, doi:10.1029/2006GL028222, 2006.

1094 Norris, D. K.: Geology of the northern Yukon and northwestern District of Mackenzie. Geological Survey
 1095 of Canada, Map 1581A, scale 1:500 000, 1984.

1096 O’Donnell, J. A., Aiken, G. R., Kane, E. S., and Jones, J. B.: Source water controls on the character and
 1097 origin of dissolved organic matter in streams of the Yukon River basin, Alaska, *J. Geophys. Res.*
 1098 *Biogeosciences*, 115, 1–12, doi:10.1029/2009JG001153, 2010.

1099 Olefeldt, D., Goswami, S., Grosse, G., Hayes, D., Hugelius, G., Kuhry, P., McGuire, A. D., Romanovsky, V.
 1100 E., Sannel, A. B. K., Schuur, E. A. G., and Turetsky, M. R.: Circumpolar distribution and carbon storage of
 1101 thermokarst landscapes, 7, 13043, 2016.

1102 Palstra, S. and Meijer, H.: Biogenic carbon fraction of biogas and natural gas fuel mixtures determined
 1103 with ¹⁴C, *Radiocarbon*, 56, 7–28, doi:10.2458/56.16514, 2014.

1104 Pinheiro, J., Bates, D., DebRoy, S., Sarkar, D., and R Core Team: nlme: Linear and nonlinear mixed effects
 1105 models. R package version 3.1-120, <http://CRAN.R-project.org/package=nlme>., 2015.

1106 Poulin, B. A., Ryan, J. N., and Aiken, G. R.: Effects of iron on optical properties of dissolved organic
 1107 matter, *Environ. Sci. Technol.*, 48, 10098–10106, doi:10.1021/es502670r, 2014.

1108 Prokushkin, A. S., Kajimoto, T., Prokushkin, S. G., McDowell, W. H., Abaimov, A. P., and Matsuura, Y.:
 1109 Climatic factors influencing fluxes of dissolved organic carbon from the forest floor in a continuous-
 1110 permafrost Siberian watershed, *Can. J. For. Res.*, 35, 2130–2140, doi:10.1139/x05-150, 2005.

1111 Pumpanen, J., A. L., Heli, M., Kolari, P., Ilvesniemi, H., Mammarella, I., Hari, O., Nikinmaa, E., Heinonsalo,
 1112 J., Back, J., Ojala, A., Berninger, F., and Vesala, T.: Precipitation and net ecosystem exchange are the
 1113 most important drivers of DOC flux in upland boreal catchments, *J. Geophys. Res. Biogeosciences*, 119,
 1114 1861–1878, doi:10.1002/2014JG002705, 2014.

1115 Qualls, R. and Haines, B. L.: Measuring adsorption isotherms using continuous, unsaturated flow through
 1116 intact soil cores, *Soil Sci. Soc. Am. J.*, 56, 456–460, doi:10.2136/sssaj1992.03615995005600020019x,
 1117 1992.

Deleted: McGuire, A. D., Anderson, L. G., Christensen, T. R., Dallimore, S., Guo, L., Hayes, D. J., Heimann, M., Lorenson, T. D., MacDonald, R. W. and Roulet, N.: Sensitivity of the carbon cycle in the Arctic to climate change, *Ecol. Monogr.*, 79, 523–555, doi:10.1890/08-2025.1, 2009.¶

1123 R Core Team: R: A Language and Environment for Statistical Computing, R Foundation for Statistical
1124 Computing, Vienna, Austria. <http://www.r-project.org/>, 2015.

1125 Rampton, V. N.: Quaternary geology of the Tuktoyaktuk coastlands, Northwest Territories, Geol. Surv.
1126 Canada, 1988.

1127 Romanovsky, V. E., Smith, S. L., and Christiansen, H. H.: Permafrost thermal state in the polar Northern
1128 Hemisphere during the international polar year 2007–2009: a synthesis, *Permafrost Periglacial Process.*,
1129 21, 106–116, doi: 10.1002/ppp.689, 2010.

1130 Schuur, E., Bockheim, J., Canadell, J. G., Euskirchen, E., Field, C. B., Goryachkin, S. V., Hagemann, S.,
1131 Kuhry, P., Lafleur, P. M., Lee, H., Nelson, M. F. E., Rinke, A., Romanovsky, V. E., Shiklomanov, N.,
1132 Tarnocai, C., Venevsky, S., Vogel, J. G., and Zimov, S. A.: Vulnerability of permafrost carbon to climate
1133 change : Implications for the global carbon cycle, *Bioscience*, 58, 701–714, doi:10.1641/B580807, 2008.

1134 Schuur, E. A. G., Abbott, B. W., Bowden, W. B., Brovkin, V., Camill, P., Canadell, J. G., Chanton, J. P.,
1135 Chapin, F. S., Christensen, T. R., Ciais, P., Crosby, B. T., Czimczik, C. I., Grosse, G., Harden, J., Hayes, D. J.,
1136 Hugelius, G., Jastrow, J. D., Jones, J. B., Kleinen, T., Koven, C. D., Krinner, G., Kuhry, P., Lawrence, D. M.,
1137 McGuire, A. D., Natali, S. M., O'Donnell, J. A., Ping, C. L., Riley, W. J., Rinke, A., Romanovsky, V. E., Sannel,
1138 A. B. K., Schädel, C., Schaefer, K., Sky, J., Subin, Z. M., Tarnocai, C., Turetsky, M. R., Waldrop, M. P.,
1139 Walter Anthony, K. M., Wickland, K. P., Wilson, C. J., and Zimov, S. A.: Expert assessment of vulnerability
1140 of permafrost carbon to climate change, *Clim. Change*, 119, 359–374, doi:10.1007/s10584-013-0730-7,
1141 2013.

1142 Schuur, E. A. G., McGuire, A. D., Grosse, G., Harden, J. W., Hayes, D. J., Hugelius, G., Koven, C. D., and
1143 Kuhry, P.: Climate change and the permafrost carbon feedback, *Nature*, 520, 171–179,
1144 doi:10.1038/nature14338, 2015.

1145 Segal, R. A., Lantz, T. C., and Kokelj, S. V.: Acceleration of thaw slump activity in glaciated landscapes of
1146 the Western Canadian Arctic, *Environ. Res. Lett.*, 11, 34025, doi:10.1088/1748-9326/11/3/034025, 2016.

1147 Spencer, R. G. M., Mann, P. J., Dittmar, T., Eglinton, T. I., Mcintyre, C., Holmes, R. M., Zimov, N., and
1148 Stubbins, A.: Detecting the signature of permafrost thaw in Arctic rivers, *Geophys. Res. Lett.*, 42,
1149 doi:10.1002/2015GL063498, doi:10.1002/2015GL063498, 2015.

1150 Street, L. E., Dean, J. F., Billett, M. F., Baxter, R., Dinsmore, K. J., Lessels, J. S., Subke, J.-A., Tetzlaff, D.,
1151 and Wookey, P. A.: Redox dynamics in the active layer of an Arctic headwater catchment; examining the
1152 potential for transfer of dissolved methane from soils to stream water, *J. Geophys. Res. Biogeosci.*, 121,
1153 2776–2792, doi: 10.1002/2016JG003387, 2016.

1154 Striegl, R. G., Aiken, G. R., Dornblaser, M. M., Raymond, P. A., and Wickland, K. P.: A decrease in
1155 discharge-normalized DOC export by the Yukon River during summer through autumn, *Geophys. Res.*
1156 *Lett.*, 32, 1–4, doi:10.1029/2005GL024413, 2005.

1157 Tank, S. E., Raymond, P. A., Striegl, R. G., McClelland, J. W., Holmes, R. M., Fiske, G. J., and Peterson, B.
1158 J.: A land-to-ocean perspective on the magnitude, source and implication of DIC flux from major Arctic
1159 rivers to the Arctic Ocean, *Global Biogeochem. Cycles*, 26, GB4018, doi:10.1029/2011GB004192, 2012a.

1160 Tank, S. E., Manizza, M., Holmes, R. M., McClelland, J. W., and Peterson, B. J.: The processing and impact
1161 of dissolved riverine nitrogen in the Arctic Ocean, *Estuaries and Coasts*, 35, 401–415,
1162 doi:10.1007/s12237-011-9417-3, 2012b.

- 1163 Tanski, G., Couture, N., Lantuit, H., Eulenburg, A., and Fritz, M.: Eroding permafrost coasts release low
 1164 amounts of dissolved organic carbon (DOC) from ground ice into the nearshore zone of the Arctic Ocean,
 1165 *Glob. Biogeochem. Cycles*, 30, 1054–1068, doi:10.1002/2015GB005337, 2016.
- 1166 Tanski, G., Lantuit, H., Ruttor, S., Knoblauch, C., Radosavljevic, B., Strauss, J., Wolter, J., Irrgang, A. M.,
 1167 Ramage, J., and Fritz, M.: Transformation of terrestrial organic matter along thermokarst-affected
 1168 permafrost coasts in the Arctic. *Sci. Total Environ.* 581–582, 434–447, doi:
 1169 10.1016/j.scitotenv.2016.12.152, 2017.
- 1170 Thompson, M. S., Prowse, T. D., Kokelj, S. V., and Wrona, F. J.: The impact of sediments derived from
 1171 thawing permafrost on tundra lake water chemistry: An experimental approach, *Proc. Ninth Int. Conf.*
 1172 *Permafrost*, 29, 1763–1768, 2008.
- 1173 Vonk, J. E. and Gustafsson, Ö.: Permafrost-carbon complexities, *Nat. Geosci.*, 6, 675–676,
 1174 doi:10.1038/ngeo1937, 2013.
- 1175 Vonk, J. E., Mann, P. J., Dowdy, K. L., Davydova, A., Davydov, S. P., Zimov, N., Spencer, R. G. M., Bulygina,
 1176 E. B., Eglinton, T. I., and Holmes, R. M.: Dissolved organic carbon loss from Yedoma permafrost amplified
 1177 by ice wedge thaw, *Environ. Res. Lett.*, 8, 35023, doi:10.1088/1748-9326/8/3/035023, 2013a.
- 1178 Vonk, J. E., Mann, P. J., Davydov, S., Davydova, A., Spencer, R. G. M., Schade, J., Sobczak, W. V., Zimov,
 1179 N., Zimov, S., Bulygina, E., Eglinton, T. I., and Holmes, R. M.: High biolability of ancient permafrost carbon
 1180 upon thaw, *Geophys. Res. Lett.*, 40, 2689–2693, doi:10.1002/grl.50348, 2013b.
- 1181 Vonk, J. E., Tank, S. E., Mann, P. J., Spencer, R. G. M., Treat, C. C., Striegl, R. G., Abbott, B. W., and
 1182 Wickland, K. P.: Biodegradability of dissolved organic carbon in permafrost soils and waterways: a meta-
 1183 analysis, *Biogeosciences*, 12, 6915–6930, doi:10.5194/bg-12-8353-2015, 2015a.
- 1184 Vonk, J. E., Tank, S. E., Bowden, W. B., Laurion, I., Vincent, W. F., Alekseychik, P., Amyot, M., Billet, M. F.,
 1185 Canário, J., Cory, R. M., Deshpande, B. N., Helbig, M., Jammot, M., Karlsson, J., Larouche, J., Macmillan,
 1186 G., Rautio, M., Walter Anthony, K. M., and Wickland, K. P.: Reviews and syntheses: Effects of permafrost
 1187 thaw on Arctic aquatic ecosystems, *Biogeosciences*, 12, 7129–7167, doi:10.5194/bg-12-7129-2015,
 1188 2015b.
- 1189 Ward, R. C. and Robinson, M.: Principles of Hydrology, Fourth Edition, McGraw-Hill International (UK)
 1190 Limited., 2000.
- 1191 Watanabe, S., Laurion, I., Chokmani, K., Pienitz, R., and Vincent, W. F.: Optical diversity of thaw ponds in
 1192 discontinuous permafrost: A model system for water color analysis, *J. Geophys. Res. Biogeosciences*,
 1193 116, doi:10.1029/2010JG001380, 2011.
- 1194 Weishaar, J. and Aiken, G.: Evaluation of specific ultra-violet absorbance as an indicator of the chemical
 1195 content of dissolved organic carbon, *Environ. Chem.*, 37, 4702–4708, doi:10.1021/es030360x, 2003.
- 1196 Woods, G. C., Simpson, M. J., Pautler, B. G., Lamoureux, S. F., Lafrenière, M. J., and Simpson, A. J.:
 1197 Evidence for the enhanced lability of dissolved organic matter following permafrost slope disturbance in
 1198 the Canadian High Arctic, *Geochim. Cosmochim. Acta*, 75, 7226–7241, doi:10.1016/j.gca.2011.08.013,
 1199 2011.
- 1200 Yanagihara, Y., Koike, T., Matsuura, Y., Mori, S., Shibata, H., Satoh, F., Masuyagina, O., Zyryanova, O.,
 1201 Prokushkin, A. S., Prokushkin, S. G., and Abaimov, A. P.: Soil respiration on the contrasting north- and
 1202 south-facing slopes of a larch forests in Central Siberia, *Eurasian J. For. Res.*, 1, 19–29, 2000.

Deleted: Walsh, J. E., Overland, J. E., Groisman, P. Y. and Rudolf, B.: Snow, Water, Ice and Permafrost in the Arctic (SWIPA): Climate change and the cryosphere, Arctic Monitoring and Assessment Programme (AMAP), Oslo, Norway., 2011.¶

- 1207 Zeileis, A. and Grothendieck, G.: zoo: S3 infrastructure for regular and irregular time series, *J. Stat.*
1208 *Softw.*, 14, 1–27, 2005.
- 1209 Zeileis, A. and Hothorn, T.: Diagnostic checking in regression relationships., *R News*, 2, 7–10, 2002.
- 1210 Zhou, Y., Guo, H., Lu, H., Mao, R., Zheng, H., and Wang, J.: Analytical methods and application of stable
1211 isotopes in dissolved organic carbon and inorganic carbon in groundwater, *Rapid Commun. Mass*
1212 *Spectrom.*, 29, 1827–1835, doi:10.1002/rcm.7280, 2015.
- 1213 Zuur, A. F., Ieno, E. N., Walker, N., Saveliev, A. A., and Smith, G. M.: *Mixed Effects Models and Extensions*
1214 *in Ecology with R*, Springer, New York., 2009.
- 1215

1216 **Table 1:** Slump characteristics and sampling information for eight retrogressive thaw slumps sampled
 1217 during the 2014 field season on the Peel Plateau, NWT, Canada. Characteristics are derived from
 1218 published values and field estimations.

Slump location	Sample dates (Julian day) ^a	Latitude	Longitude	Area (ha)	Debris tongue (m) ^b	Headwall height (m)
FM4	202, 210, 223	67 16.679	-135 09.573	8.8	960	16 to 20 ^d
FM2	200, 209, 222	67 15.462	-135 14.216	31.7	1529	25 ^e
FM3	197, 212	67 15.100	-135 16.270	6.1	576	10 ^e
SD	196, 213, 234	67 10.818	-135 43.630	3.3	NA	2 – 4 ^d
HA	190, 229	67 09.057	-135 41.121	5.9	288	6 – 10 ^d
HB	190, 229	67 14.397	-135 49.167	13.6 ^c	257	6 – 10 ^d
HC	190, 229	67 19.652	-135 53.620	10.3, 10.3 ^c	408	6 – 10 ^d
HD	190, 229	67 24.025	-135 20.048	1.8	137	6 – 10 ^d
Weather Station		67 14.756	-135 12.920			

1219
 1220 ^a Excludes samples for the FM3 ‘environmental controls’ analysis which was conducted on 17 additional
 1221 dates; HD, Julian date 229 did not include a within-slump sample.
 1222 ^b The length of debris tongue measured from the base of the debris scar, along the valley bottom stream
 1223 ^c Site HB is comprised of two smaller slump features that have merged into the scar zone delineated
 1224 here; site HC is comprised of 5 separate slump features that have merged into two scar zones, each with
 1225 an area of 10.3 ha
 1226 ^d Rough estimates by field crews over 2014 and 2015 field seasons
 1227 ^e (Kokelj et al., 2015)
 1228
 1229
 1230

1231 **Table 2:** Results of the mixed-effects models used to assess the effects of slumping on stream water
 1232 chemistry and optical characteristics. Downstream models incorporated data from downstream and
 1233 upstream sites; within-slump models incorporated data from within-slump and upstream sites. Provided
 1234 are degrees of freedom (df), t-statistics, and p-values for individual model runs. Further details on the
 1235 statistical approach are provided in Section 3.4.
 1236

	Downstream			Within-slump		
	df	t	p	df	t	p
DOC	20	-12.895	<.0001	30	-1.468	0.153
Na	33	9.662	<.0001	30	7.278	0.000
Ca	33	9.767	<.0001	30	4.782	0.000
Mg	33	6.166	<.0001	30	8.593	0.000
Conductivity	32	43.083	<.0001	30	11.895	0.000
TSS	29	6.692	<.0001	28	2.187	0.037
SUVA	31	-5.296	<.0001	30	-35.052	0.000
S _R	31	5.092	<.0001	31	8.065	0.000
S ₂₇₅	30	2.695	0.011	31	8.159	0.000
S ₃₅₀	31	-3.595	0.001	31	16.665	0.000

1237

1238

1239 **Table 3:** Measured fraction modern carbon ($F^{14}C$) and estimated calendar years before present for ^{14}C of
 1240 dissolved organic carbon samples collected upstream of, and within drainage waters of, selected slump
 1241 sites. Data were collected during the summer of 2016. nc indicates sample not collected. Error
 1242 estimates indicate 1 σ .

1243

Site	$F^{14}C$		^{14}C yr BP	
	Upstream	Within-slump	Upstream	Within-slump
FM4	0.9734 ± 0.0029	nc	217 ± 24	nc
FM2	0.9764 ± 0.0032	0.3030 ± 0.0024	192 ± 27	9592 ± 64
FM3	1.0023 ± 0.0030	0.3618 ± 0.0018	modern	8167 ± 39
SD	1.0216 ± 0.0035	0.8659 ± 0.0025	modern	1157 ± 23

1244

1245 **Table 4:** Results of multiple linear regression analyses to assess environmental controls on upstream and downstream DOC flux, and upstream
 1246 and downstream DOC concentration. nr indicates variables that were not retained in the best fit regression model; NA indicates variables that
 1247 were not run in individual analyses. Significant p-values are indicated with bold text; marginal results ($0.05 < p < 0.10$) are indicated in italics.
 1248 Model statistics are as follows: downstream flux $r^2=0.84$, $F_{7,11}=8.25$, $p = 0.001$; upstream flux $r^2=0.87$, $F_{7,11}=10.79$, $p < 0.001$; downstream
 1249 concentration $r^2=0.85$, $F_{4,14}=19.57$, $p < 0.001$; upstream concentration $r^2=0.91$, $F_{5,13}=27.05$, $p < 0.001$.

Coefficient	Downstream DOC flux			Upstream DOC flux			Downstream DOC concentration			Upstream DOC concentration		
	Estimate	t	p	Estimate	t	p	Estimate	t	p	Estimate	t	p
Average Air Temperature (°C)												
0 h	-67.08	-1.685	0.120	-115.96	-3.286	0.007	nr	nr	nr	0.165	2.349	0.035
48 h	nr	nr	nr	56.32	1.534	0.153	0.332	6.886	<0.001	0.396	5.510	<0.001
72 h	-95.15	-2.594	0.025	-94.17	-2.717	0.020	nr	nr	nr	nr	nr	nr
120 h	nr	nr	nr	nr	nr	nr	0.134	3.527	0.003	0.203	4.411	<0.001
Rainfall (mm)												
0h	116.13	5.411	<0.001	105.47	6.039	<0.001	<i>-0.066</i>	<i>-1.967</i>	<i>0.069</i>	nr	nr	nr
48h	nr	nr	nr	nr	nr	nr	nr	nr	nr	nr	nr	nr
72h	nr	nr	nr	nr	nr	nr	nr	nr	nr	nr	nr	nr
120h	<i>-23.94</i>	<i>-1.970</i>	<i>0.075</i>	-24.15	-2.529	0.028	nr	nr	nr	nr	nr	nr
Average net radiation (W m⁻²)												
0h	4.96	1.286	0.225	nr	nr	nr	-0.021	-4.043	0.001	-0.021	-3.387	0.005
48h	nr	nr	nr	nr	nr	nr	nr	nr	nr	nr	nr	nr
72h	5.58	1.545	0.151	4.04	1.563	0.146	nr	nr	nr	nr	nr	nr
120h	nr	nr	nr	nr	nr	nr	nr	nr	nr	nr	nr	nr
Total suspended sediment (mg L⁻¹)												
Downstream	<i>-0.02</i>	<i>-2.102</i>	<i>0.059</i>	NA	NA	NA	nr	nr	nr	NA	NA	NA
Upstream	NA	NA	NA	-0.32	-1.626	0.132	NA	NA	NA	-0.0006	-1.627	0.128

1250 **Figure captions:**

1251 **Fig. 1: Location and morphology of thaw slumps on the Peel Plateau, Northwest Territories, Canada.**

1252 Panel A depicts the stream networks and location of the eight retrogressive thaw slumps studied. Panel
1253 B depicts representative sampling locations at each slump site; FM3 depicted. Panels C-E depict
1254 representative thaw-slump headwall stratigraphies. Panel C shows a mega-slump (FM3, the smallest
1255 mega-slump, is depicted); panel D shows a moderate-sized slump (HB); panel E shows the smallest
1256 slump that was sampled (SD). In panels C and D, the approximate location of the modern active layer (a),
1257 early Holocene-aged relict active layer (b), and Pleistocene-aged glacialic materials (c) is shown.

Deleted: on the Peel Plateau, Northwest Territories, Canada

1258 **Fig. 2:** The effect of retrogressive thaw slumps on stream water dissolved organic carbon (DOC)
1259 concentration. Each data point represents the mean and standard error of measurements across all
1260 sampling dates, as described in Table 1. The bottom two panels show the ratio of within-slump:
1261 upstream, and downstream: upstream DOC concentrations within individual slumps, with points
1262 indicating the mean and standard error of this ratio across sample dates.

1263 **Fig. 3:** Box and whisker plots to illustrate the effects of retrogressive thaw slump activity on stream
1264 geochemistry. Each boxplot includes data from across all slumps and sampling periods, and indicates
1265 median values, 25th and 75th percentiles (box extremities), 10th and 90th percentiles (whiskers), and
1266 outlier points. U=upstream sites; W=within-slump sites; D=downstream sites.

1267 **Fig. 4:** The effect of retrogressive thaw slumps on the optical properties of stream water dissolved
1268 organic matter. Each data point represents the mean and standard error of measurements across all
1269 sampling dates, as described in Table 1. Shown are specific UV absorbance (SUVA₂₅₄), spectral slopes
1270 between 275-295 and 350-400 nm (S₂₇₅₋₂₉₅; S₃₅₀₋₄₀₀) and the slope ratio (S_R).

Formatted: Subscript

Formatted: Subscript

Formatted: Subscript

Formatted: Subscript

1271 **Fig. 5:** Paired oxygen isotopic ($\delta^{18}\text{O}$ ‰) and SUVA₂₅₄ (L mg C⁻¹m⁻¹) data, to demonstrate the relationship
1272 between source water age and dissolved organic matter composition. Reference $\delta^{18}\text{O}$ values are from
1273 Lacelle et al. (2013): the modern active layer value is derived from active layer pore water in this region,
1274 icy diamicton has been sourced as Holocene in origin, and the $\delta^{18}\text{O}$ value for Pleistocene-aged ground ice
1275 is the most positive value for this region.

Deleted: s

Deleted: is equivalent of the meteoric water line

Formatted: Not Highlight

Deleted: is

Deleted: been aged to be

Deleted: era

Deleted: enriched

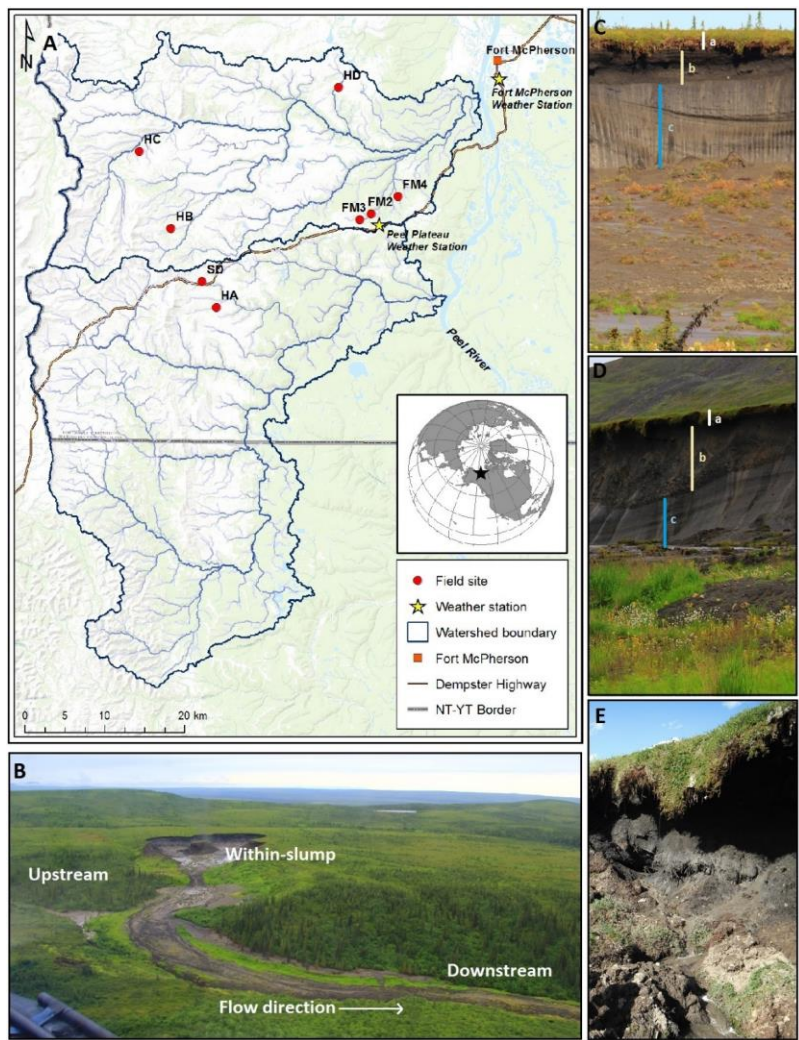
Deleted: Pleistocene-aged

1276 **Fig. 6:** Environmental conditions (solar radiation, precipitation and mean daily air temperature) and DOC
1277 flux upstream and downstream of slump FM3 across a month-long sample period (July 12-August 12,
1278 2014). Corresponding multiple linear regressions are described in Table 4.

1279 **Fig. 7:** Within-slump fluxes of dissolved organic carbon (DOC), and TSS, compared to the calculated
1280 (downstream - upstream) fluxes for these two constituents. TSS – a conservative tracer over short
1281 distances – shows an additive response where the measured within-slump flux is equivalent to the
1282 calculated (downstream - upstream) flux. In contrast, DOC shows clear evidence of downstream loss.

1283

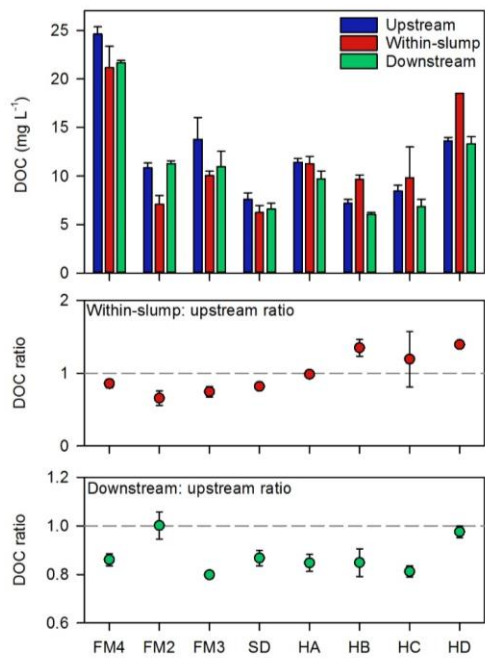
1284



1293
 1294 **Fig. 1:** Location and morphology of thaw slumps on the Peel Plateau, Northwest Territories, Canada.
 1295 Panel A depicts the stream networks and location of the eight retrogressive thaw slumps studied. Panel
 1296 B depicts representative sampling locations at each slump site; FM3 depicted. Panels C-E depict
 1297 representative thaw-slump headwall stratigraphies. Panel C shows a mega-slump (FM3, the smallest
 1298 mega-slump, is depicted); panel D shows a moderate-sized slump (HB); panel E shows the smallest
 1299 slump that was sampled (SD). In panels C and D, the approximate location of the modern active layer (a),
 1300 early Holocene-aged relict active layer (b), and Pleistocene-aged glacial materials (c) is shown.

1301

Deleted: Figure 1 ¶

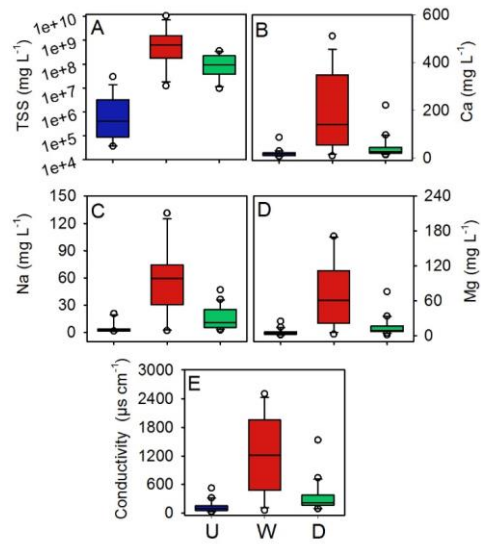


1302

1303 **Fig. 2:** The effect of retrogressive thaw slumps on stream water dissolved organic carbon (DOC)
 1304 concentration. Each data point represents the mean and standard error of measurements across all
 1305 sampling dates, as described in Table 1. The bottom two panels show the ratio of within-slump:
 1306 upstream, and downstream: upstream DOC concentrations within individual slumps, with points
 1307 indicating the mean and standard error of this ratio across sample dates.

1308

Deleted: Figure 2 ¶

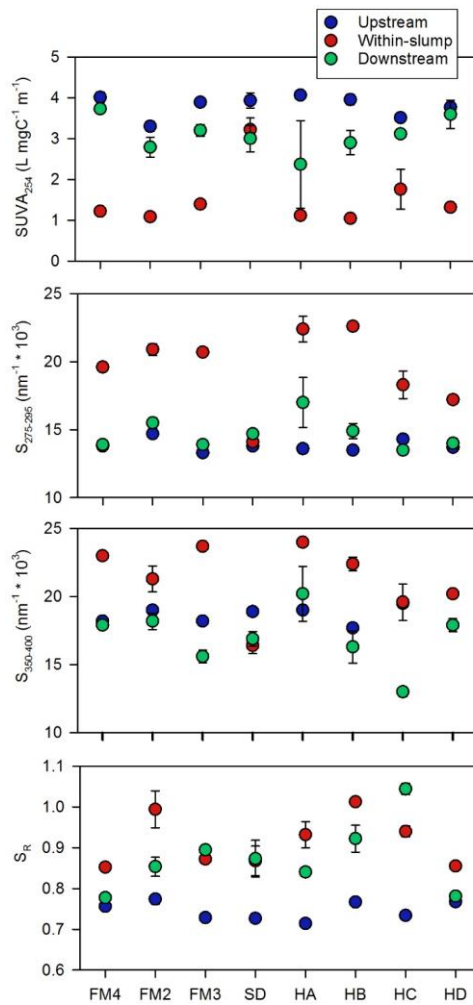


1311

1312 **Fig. 3:** Box and whisker plots to illustrate the effects of retrogressive thaw slump activity on stream
 1313 geochemistry. Each boxplot includes data from across all slumps and sampling periods, and indicates
 1314 median values, 25th and 75th percentiles (box extremities), 10th and 90th percentiles (whiskers), and
 1315 outlier points. U=upstream sites; W=within-slump sites; D=downstream sites.

1316

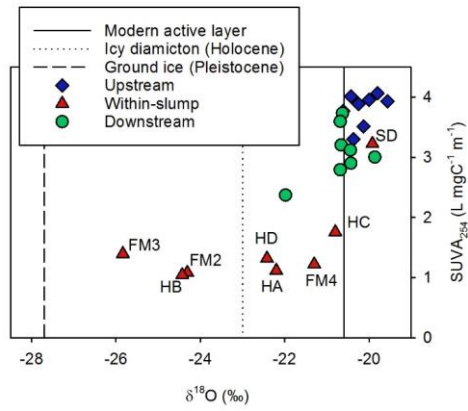
Deleted: Figure 3 ¶



1319 **Fig. 4:** The effect of retrogressive thaw slumps on the optical properties of stream water dissolved
 1320 organic matter. Each data point represents the mean and standard error of measurements across all
 1321 sampling dates, as described in Table 1. Shown are specific UV absorbance (SUVA₂₅₄), spectral slopes
 1322 between 275-295 and 350-400 nm (S₂₇₅₋₂₉₅; S₃₅₀₋₄₀₀) and the slope ratio (S_R).

1323

Deleted: Figure 4 ¶

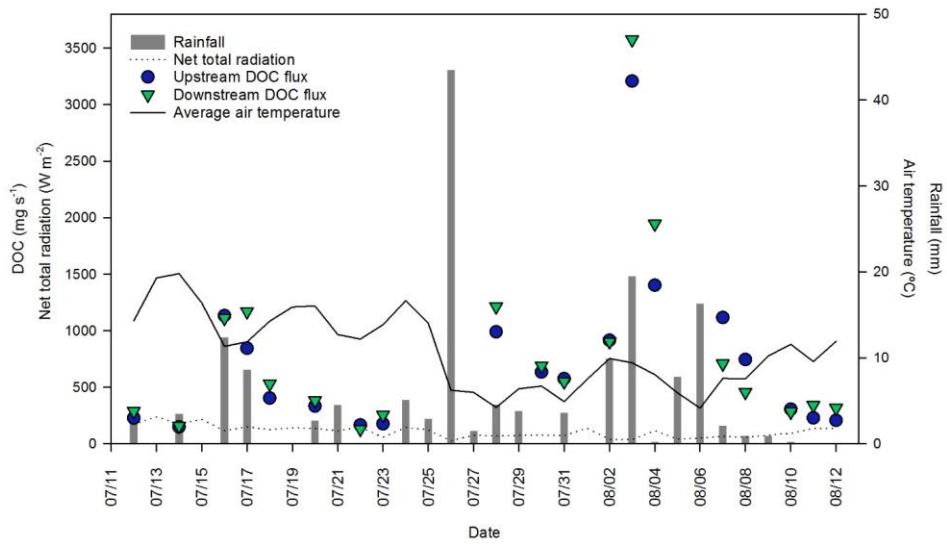


1325

1326 **Fig. 5:** Paired oxygen isotopic ($\delta^{18}\text{O}$ ‰) and SUVA_{254} ($\text{L mg C}^{-1}\text{m}^{-1}$) data, to demonstrate the relationship
 1327 between source water age and dissolved organic matter composition. Reference $\delta^{18}\text{O}$ values are from
 1328 Lacelle et al. (2013): the modern active layer value is derived from active layer pore water in this region,
 1329 icy diamicton has been sourced as Holocene in origin, and the $\delta^{18}\text{O}$ value for Pleistocene-aged ground ice
 1330 is the most positive value for this region.

1331

Deleted: Figure 5 ¶

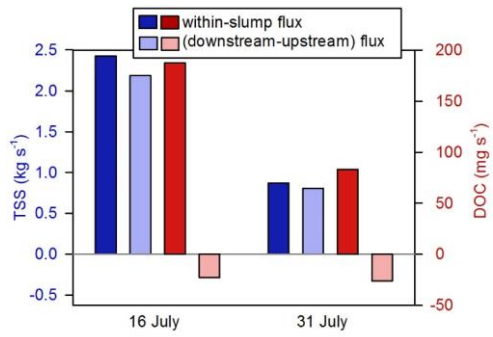


1333

1334 **Fig. 6:** Environmental conditions (solar radiation, precipitation and mean daily air temperature) and DOC
 1335 flux upstream and downstream of slump FM3 across a month-long sample period (July 12-August 12,
 1336 2014). Corresponding multiple linear regressions are described in Table 4.

1337

Deleted: Figure 6 ¶



1339

1340

1341 **Fig. 7:** Within-slump fluxes of dissolved organic carbon (DOC), and TSS, compared to the calculated
 1342 (downstream - upstream) fluxes for these two constituents. TSS – a conservative tracer over short
 1343 distances – shows an additive response where the measured within-slump flux is equivalent to the
 1344 calculated (downstream - upstream) flux. In contrast, DOC shows clear evidence of downstream loss.

1345

Deleted: Figure 7